IEEE Access
Multidisciplinary ⋮ Rapid Review ⋮ Open Access Journal

Received November 11, 2020, accepted November 22, 2020, date of publication November 25, 2020,
date of current version December 9, 2020.

Digital Object Identifier 10.1109/ACCESS.2020.3040624

Rainfall and Diffraction Modeling for Millimeter-Wave Wireless Fixed Systems

ZAID AHMED SHAMSAN, (Senior Member, IEEE)
Department of Electrical Engineering, College of Engineering, Al Imam Mohammad Ibn Saud Islamic University, Riyadh 11432, Saudi Arabia
Department of Communication and Computer Engineering, Faculty of Engineering and Information Technology, Taiz University, Taiz 6803, Yemen
e-mail: shamsan@ieee.org

ABSTRACT Rain attenuation is the main practical problem that confronts wireless signals specifically when it uses millimeter-waves for fifth-generation (5G) communication systems. In addition, due to that the urban environments are characterized by many high buildings act as diffraction objects can block the signal path and produce non-line of sight (NLOS) situations. These diffraction materials can cause further considerable losses that disturb the received power at the 5G receiver. This paper proposes a new model can investigate the influence of both precipitation and diffraction phenomena on wireless point to point (PPT) communication systems. This new research work utilizes measured rainfall data and actual scenarios in an urban environment to simulate the wireless PPT system and examine the influence of rainfall and knife-edge diffraction (KED) on the performance of the PPT system and signal strength at the receiver. Several durations of exceedances of rain rates and various operation scenarios have been employed to study and analyze the status of 5G wireless system links. The results indicated that there is an exchange of the effect of rain and KED diffraction in the lower millimeter-waves compared to the higher millimeter-waves. This study declares that at higher frequency bands the rain attenuation is observed to be greater, the diffraction loss is higher, and the path loss is also larger compared to the effect of these three factors seen at lower frequency bands. Furthermore, specific carrier frequencies, as in the case of 60 GHz, undergo extra huge atmospheric absorption loss which can diminish the communication coverage of the PPT system link.

INDEX TERMS Rain rate, rain attenuation, millimeter-waves, KED mechanism, antenna height, 5G, receiver sensitivity, received power, wireless fixed link.

I. INTRODUCTION

Due to the shortage in frequency spectrum allocated to 4G wireless communication system operating at lower frequencies than 6 GHz, several frequency bands have been added and the frequency spectrum has been extended to millimeter-waves (mmWaves) so as to support 5G communication system with a countless number of services that need much bandwidth to deliver high data rate to the end-user [1]. Different mmWave frequency bands can be utilized for different situations such as backhaul and fixed wireless access (FWA) to offer fast speed communication for numerous applications [2]. Practically, the 5G wireless system has been initiated in the frequency range 1 (FR1) which covers frequency band less than 6 GHz, however, FR2 which covers millimeter-waves is still under standardization by the third generation partnership project (3GPP). On the other hand, mmWaves are suffering from higher attenuation, compared to lower bands, due to the effect of energy absorption and scattering by meteorological conditions such as rainfall, fog, snow, humidity, etc. That is, the frequency bands above 10 GHz, rainfall attenuation either for terrestrial links [3] or satellite links [4] is the predominant influence particularly in tropical regions such as Malaysia, Brazil, Nigeria, and other analogous areas in Europe that have similar weather conditions. This attenuation influences the communication link quality and then significantly reduces system performance [4], [5].

The radio channel propagation conditions play an essential role to fulfill the minimum requirements for wireless service availability. The precipitation attenuation in mmWaves, particularly in E-band which ranges from 60 GHz to 90 GHz and have very short wavelengths from 3.33 mm to 5 mm, is a key impairment among other propagation condition factors to consider for realizing communication service quality

The associate editor coordinating the review of this manuscript and approving it for publication was Ahmed Farouk.

requirements. Additionally, mmWaves are obviously unable to penetrate barriers or materials, and the hardware components operating at mmWave wavelengths, for example analog to digital converters, are not cost-effective [6]. Moreover, previous studies such as [7] showed that higher frequencies have a tendency to be influenced by rainfall attenuation more willingly than multipath which is a phenomenon takes place with lower frequencies. Furthermore, the rainfall attenuation at the higher frequencies is highly serious specifically in tropical weather regions [8].

Several models of the International Telecommunication Union- Radiocommunication sector (ITU-R) [9]–[12] for precipitation attenuation prediction have been developed to make sure that wireless radio links satisfy the standard and acceptable constraints. These ITU-R models were designed for conventional microwave frequency bands and worldwide proved high efficiency in diverse times and areas [13]–[16].

In addition to the abovementioned signal impairments, signal fading loss caused by a knife-edge diffraction (KED) mechanism is another factor that can influence signal propagation, but a recent study [17] has been conducted between dust storms and diffraction mechanism. However, no previous studies combine diffraction with rainfall attenuation even the new Matlab-based channel simulator named NYUSIM, which is being developed by New York University (NYU) and NYU WIRELESS center, does not include the diffraction model in the simulation procedures [18].

In this regard, Riyadh city where real scenarios for the current paper have been proposed, its building structure gets taller quickly and many towers and high-rise buildings are distributed here and there inside the city. These constructions impose the effect of change in the coverage scenarios and convert communication links from line of sight (LOS) into non-line of sight (NLOS) conditions due to signal blocking caused by diffraction objects such as these tall buildings. The diffraction effects must be carefully considered and its consequences on connection links should be examined [18]. For this purpose, ITU-R P.526-14 [18] and ITU-R P.530 [9]–[12], [20] recommendations have been agreed to provide propagation prediction. Where, ITU-R P.526-14 recommendation offerings a number of models to estimate the influence of KED blockage styles on strength of the signal power at the receiver in various path geometries [19]. Furthermore, ITU-R P.530 series offers estimation schemes for effects of the signal propagation on static LOS connection link design, and also it provides tips on communication links can be designed in order to improve propagation link and reduce its losses [20].

This article develops a new model can predict attenuation losses induced by rainfall together with the effect of the KED phenomenon on the link performance. After that, we recommend techniques to improve the link performance. Even though the suggested model in this paper has been accomplished for a lonely transmitter (Tx) and receiver (Rx) antenna, it can be realized utilizing a group of antennas (multiple input multiple output (MIMO) technology) at each Tx/Rx side equipped with beamforming technology to focus the signal energy into the exact Rx. This procedure has been carried out for the purpose of studying the link situation under the effect of both rain attenuation and diffraction mechanism. As far as we know, no similar model or study combines rain and KED losses prediction has been carried out till now. Nevertheless, MIMO technology represents one of the most important tools to enhance 5G system for well heritage point to point (PPT) link operating [21]. In PPT MIMO, each individual antenna on the Tx associate with only one antenna on the Rx. In addition, the Tx and the Rx are equipped with an adequate number of antennas to rise the data rate with no need to expand the system bandwidth. According to [22], [23], usually frequency-flat and slow fading channels are assumed for PPT systems. Though, mmWaves or high frequency bands require determination of the maximum coverage of the transmitter. Moreover, involving massive-MIMO technology may highly lead point to multipoint (PMP) fixed wireless services (FWS) to be cost-effective and decrease mobile backhaul network size in contrast to the PPT system [24]–[26].

According to the previous studies, the findings from this paper present at least three contributions to the current literature which are as follows:

- First, to the best of our knowledge, no modeling work has been performed to study a PPT wireless system affected by KED mechanism together with rainfall attenuation to estimate the propagation effects on the communication link.
- Second, this modelling work mainly depends on actual rainfall readings and also actual scenarios of the urban area in Riyadh city (Saudi Arabia) which makes it more technically sound.
- Third, we investigate the combined effect of rain attenuation and KED effects for a wide range of 5G frequency bands in mmWaves. In addition, even though this paper mainly depends on communication between one Tx antenna to another Rx antenna, the design can also be developed to include a large MIMO antennas system that makes it appropriate for performing propagation prediction for the massive 5G and 6G systems with attaching some amendments associated with proposed scenarios particularly on radio covering distance and operating frequencies.

This article is organized as follows. Section II provides a detailed explanation of the proposed model to perform this propagation prediction study. In Section III, the PPT system characteristics, specifications, and parameters are offered. Various number of results for the PPT wireless system are obtained, discussed, and analyzed in Section IV. Our conclusions are drawn in Section V.

II. THE PROPOSED MODEL

It is assumed that Riyadh city, Saudi Arabia, is the proposed scenario environment. Riyadh is a modern city located above sea level (asl) by 612 m as an average. It is proposed that the wireless communication PPT link takes place in a dense

FIGURE 1. The geographical area map in Riyadh, Saudi Arabia for the proposed 9.4 km PPT radio link PSS (Tx) - KAFD (Rx), and the diffraction object (KT) is shown between the two sites.

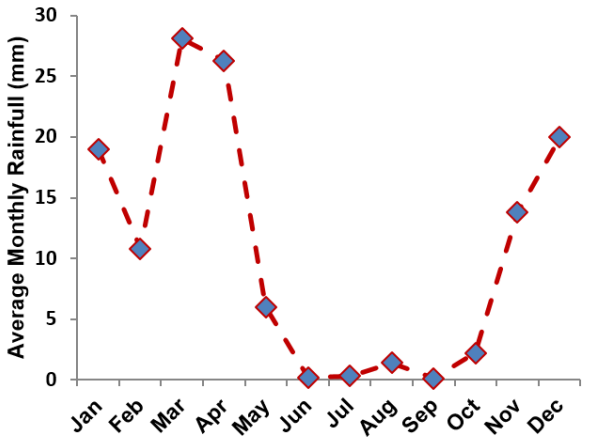

FIGURE 2. Average monthly Rainfall rate (mm) in Riyadh.

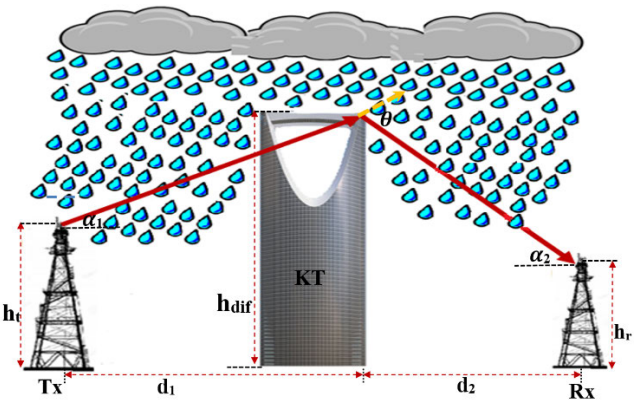

FIGURE 3. The proposed PPT model experiences rainfall attenuation and diffraction losses.

urban zone where the city is overfilled by high buildings and towers. Currently, the Kingdom Tower (KT) which is traditionally called Al-Mamlaka tower is the highest tower in Riyadh. In this paper, the King Abdullah Financial District (KAFD) is proposed to be a fixed receiver station (Rx) at a level of 623.7 m (asl) and geographically it is located in the north direction to the kingdom tower at latitude and longitude of 24.957278° and 46.699402°, correspondingly, as shown in Fig. 1. While, the Tx is assumed to be on several locations to the south direction of the KT building, where a point on Prince Sultan Street (PSS) is set as a maximum point from the KT building and allocated at latitude and longitude of 24.69124157° and 46.69343948°, respectively. This means that, in each time, the KT building (with latitude and longitude of 24.71136331° and 46.67436630°, respectively) is always in between the transmitter side (a varied point) and the receiver side (a fixed point)) and therefore the KT works as a blocking material because it has a very high height and knife-edge which affect the path of the signal transmitted from the transmitter to the receiver. This proposed communication link path from the Tx to the Rx has a maximum length of 9.4 km.

Previous research works carried out on rates of rainfall in Saudi Arabia [27], [28] indicated that approximately 50% and 20-30% of all rainfall occur at intensities in excess of 20 millimeters per hour (mm/hr) and 40 mm/hr, correspondingly. On the other hand, the statistical data analysis of rainfall gathered from earth stations states that rainfall rate is varied from place to another and it also depends on time. Precisely, the practical measurement studies revealed that Riyadh city has a flat topography and considered as one of the semi-arid regions over the world [29] where rainfall deviations may be small. The statistical data of the average amount of monthly precipitation at Riyadh through the time period from 1970 to 2003 [29] displays that the Riyadh area has variable temporal rainfall. Specifically, in the two months of March and April, the maximum amount of rainfall is received, whereas, the time period of June-October is an almost dried time period as shown in Fig. 2.

As a result, it can be noted that (i) the propagation condition in Riyadh city can be under the effect of medium rainfall rates and (ii) as it is being one of the modern areas characterized by tall towers. Therefore, the communication system feasibly suffers rain attenuation and KED losses. Thus, such a position can be modeled as in Fig. 3 which will be our main application in this paper.

A. RAINFALL DATA SOURCE AND COLLECTION METHODOLOGY

Rainfall rates in Riyadh have been collected from [30], [31], as shown in Fig. 4. This measured data has been extracted based on 18-year rainfall data collected during the time period

TABLE 1. An example: Rainfall data conversion into rain rate [30], [31].

Date	Parameter	Observation time (T)						
		10 min	20 min	30 min	1 hr	2 hrs	3 hrs	6 hrs
		10 min	20 min	30 min	60 min	120 min	180 min	360 min
May 9	I_R (mm)	8	10	10	11.5	11.5	11.5	11.5
	R (mm/h)	48	30	20	11.5	5.75	3.83	1.92

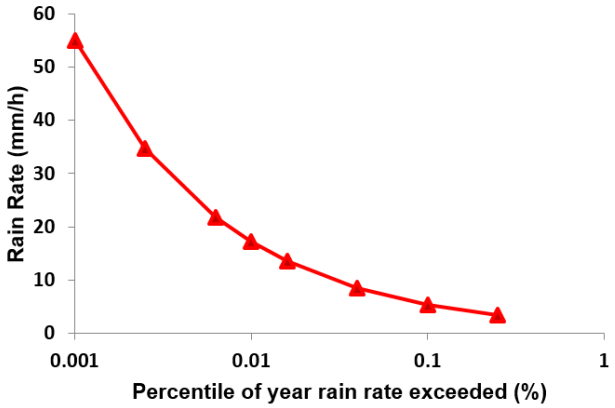

FIGURE 4. Rain rate (mm/h) in Riyadh.

from 1963 to 1980 [30], [31]. Despite the fact that this rainfall data in Riyadh is published in 1986, it can be accepted since statistics rainfall data have been published in [32] declared that irrespective of rainfall season, there is no clear change of rainfall rate for any particular year for the three decades during the period 1979–2009. This result means that the adopted rainfall data in this paper is still valid at the present time.

This accessible rainfall data [30], [31] has been individually collected from 137 recording rainfall stations/gauges scattered throughout Saudi Arabia for the period 1963-1980. Some of these rainfall gauges were placed at meteorological data-collecting sites while the rest were situated in distributed areas. The rainfall intensities, in mm, were collected by the hydrology division, ministry of agriculture and water (MAW), Saudi Arabia, and rain gauges have been utilized to record each individual storm data as a continuous rain chart for each recording rainfall station. This chart represents the maximum incremental rainfall that fell during the following time intervals: 10, 20, and 30 minutes, and 1, 2, 3, 6, and 12 hours. Total rainfall and time durations were regularly obtained for each storm. However, the available rainfall data is in mm which is not directly related to rain attenuation. Therefore, the data was transferred into the rain rate in mm/hr to be easily manipulated to obtain the rain attenuation in decibel (dB) [33], [34]. The following steps show the methodology used by [30], [31] to convert rain intensity into rain rate exceedance:

Step 1: A given maximum rainfall intensity, I_R in mm, is divided by the observation time, T in minutes (10, 20, 30, 60, etc.) for each rainfall event, so as to obtaining rain rate, R in mm/hr, by the following expression [30], [31], [35], [36]:

$$R = I_R \times \frac{60}{T} \tag{1}$$

For instance, the rainfall data in Riyadh, for May 9, 1963, can be converted as shown in Table 1.

Step 2: Assume R_e, in mm/hr, to be the rain rate exceeded, such that R_e takes certain rates of (1, 5, 10, 15, 20, . . . , etc.).

Step 3: For each event of rainfall, select a rainfall rate R and contrast it with the closest rain rate of R_e that meets the inequality: $R \geq R_e$, and take this value of R_e to be the corresponding maximum rain rate exceeded in that rain event.

Step 4: During the ith rain event: assume that the time interval T_{ie}, in minutes, in which a specified rain rate (R) exceeds R_e, equivalents to the obtaining time interval of the rainfall intensity in mm which corresponds to R.

Step 5: Obtain the time interval per year, $T(R_e)$ in minutes, for which a given R_e was exceeded, by adding all year rainfall events as follows:

$$T\ (R_e) = \sum_{i=1}^{j} T_{ie} \tag{2}$$

where j represents the total rainfall events of the year while T_{ie} represents the time interval for the ith rainfall event in which a given R_e was exceeded.

Step 6: Obtain the time interval per average year, T_{av} in minutes, for which R_e was exceeded as follows:

$$T_{av} = \frac{T\ (R_e)}{Y_r} \tag{3}$$

where Y_r is the number of recording years.

On the other hand, for several reasons, it was found that some rainfall events have been missed which can cause unreliable results. Therefore, prior processing the whole data set, the missing rainfall event data were approximated using the method of the least square which is usually used to obtain the best fit curve that represents the measured rainfall intensities [31]. Moreover, the collected rain intensity data from the MAW is subject to errors either due to human mistake during picking the rainfall intensity from the continuous graph of rain gauge, or during entering the data into the computer, or due to failure of equipment. Consequently, a computer program was utilized to examine the data consistency and execute correction whenever it needs. That is, every event of the given data the rainfall rate records, in mm/hr, were checked to make sure that rain rate data is consistent. In the case of an error has been detected, the linear interpolation method is applied to correct the record [31].

In Fig. 4, it can be seen that the rain rate exceeded 0.01% of the time (i. e., 52.56 minutes/year) is 17.17 mm/hr, and the maximum rainfall rate is 55.09 mm/hr for a time of 13.14 min/year, which corresponds to 0.0025% of the time. While the measured minimum rain rate in Riyadh is 3.36 mm/hr and this corresponds to a cumulative time of 21.9 hr/year. The measured values of the rain rates have

TABLE 2. The main system parameters of the PPT links [17], [24], [37], [38], [46], [47], [58], [59].

Description		Scenario 1	Scenario 2	Scenario 3	Scenario 4	Scenario 5
Operation frequency (GHz)		28	38	60	73	100
Bandwidth (GHz)				0.8		
Transmitter	power (dBm)	32	35	43.01	43.01	43.01
	Antenna gain (dB)	40.7	40.7	46.5	38	43.5
	Antenna height (m)			60		
Receiver	sensitivity (dBm)	-103	-103	-103	-103	-103
	Antenna gain (dB)	40.7	40.7	43.5	43.5	43.5
	Antenna height (m)			40		
Antenna size (m)		0.6	0.6	0.6	0.6	0.6
Waveguide losses (dB/m)				0.16		
Link distance range (km)				1 - 9.4		
Kingdom tower height (m)				302		
Urban loss (dB)		5.13	4.32	4.18	4.04	4.04
Statistical loss (dB)		6.16	6.09	6.08	6.07	6.07
Atmospheric absorption (dB/km)		negligible	negligible	negligible	10	negligible

been converted into excess rain attenuation in dB/km for different percentages of rain rate exceeded for horizontal and vertical polarization to select the worst-case scenario, and then the excess rain attenuation, in turn, has been transferred into rain attenuation in dB.

B. PPT SYSTEM LINK DESCRIPTION

The PPT system link in line with the scenario shown in Fig. 3 has been built and can be briefly explained as follows. First, the PPT communication system specifications including transmitter and receiver parameters have been determined with the assistance of Nautel Radio Coverage tool [17], [37], [38]. Second, the propagation channel is defined such that it can be considered the worst-case in which it is assumed that the signal received by the KAFD receiver antenna experiences rain attenuation and free space path loss. Then the loss induced by the diffraction mechanism is taken into account, such that the received signal power at KAFD undergoes the influence of the abovementioned three losses of propagation conditions: free space loss, rain attenuation, and diffraction losses. Finally, to judge that the link performance is acceptable, the received power $P_{r,dB}$ is compared with the sensitivity threshold of the receiver, and then the results are presented. This method can be depicted by a flow chart as in Fig. 5. The PPT system environment has been installed by defining the main connection link parameters, Tx parameters, Rx parameters, and then the propagation channel parameters effects of rain and diffraction phenomena are also integrated into the PPT communication environment. All the following parameters in Eq. (2) are considered to obtain the received signal, $P_{r,dB}$, in dB:

$$P_{r,dB} = EIRP + G_r - L_{sc} - L_{fs} - L_{ra} - L_{ked} - L_{ab} - L_o \tag{4}$$

where $EIRP$ denotes the effective isotropic radiated power which consists of the transmit power, P_t, by the power amplifier at the input of the antenna times the gain of the antenna itself, G_t. While G_r represents the receiver antenna gain and L_{sc} represents the PPT system connection losses. The channel propagation losses include rain attenuation, L_{ra}, diffraction loss, L_{ked}, absorption loss due to atmospheric components, L_{ab}, free space loss, L_{fs}, and other losses, L_o, such as statistical losses and urban losses.

The free space loss, L_{fs}, is basically based on the operation frequency of the PPT communication link signal, f in MHz, and the Tx-Rx separation distance, d in km [20].

$$L_{fs}(d, f) = 32.44 + 20\log(f) + 20\log(d) \tag{5}$$

For computing the rain attenuation, in dB, we will consider ITU-R P.530 model [20] which is expressed as follows:

$$L_{ra} = L_{sa}.d.r \tag{6}$$

where L_{sa} denotes the specific attenuation or excess rain attenuation (ERA) in dB/km, d is the actual PPT link distance, in km, and r is called the distance factor. The specific attenuation, L_{sa}, is given by:

$$L_{sa} = k.RR^{\alpha} \tag{7}$$

and it is calculated for the 99.99% link availability, RR, in mm/h, for the preferred region and time period, whereas k and α are the appropriate regression coefficients for the operation frequency and the used polarization as given in ITU-R model Tables [39]–[41]. These coefficients are computed as follows:

$$k = \frac{k_H + k_V + (k_H - k_V)\cos^2\vartheta\cos 2\tau}{2} \tag{8}$$

$$\alpha = \frac{k_H\alpha_H + k_V\alpha_V + (k_H\alpha_H - k_V\alpha_V)\cos^2\vartheta\cos 2\tau}{2k} \tag{9}$$

where ϑ denotes the elevation angle of the path and τ is the polarization tilt angle relative to the horizontal (it is 90°, 45°, and 0° for vertical, circular, and horizontal polarization,

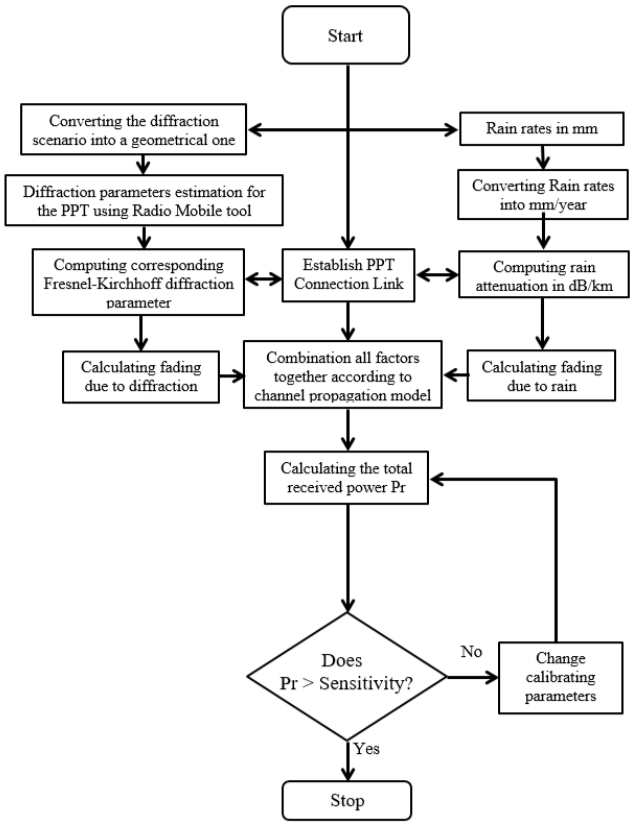

FIGURE 5. The designed flow chart for the proposed PPT model.

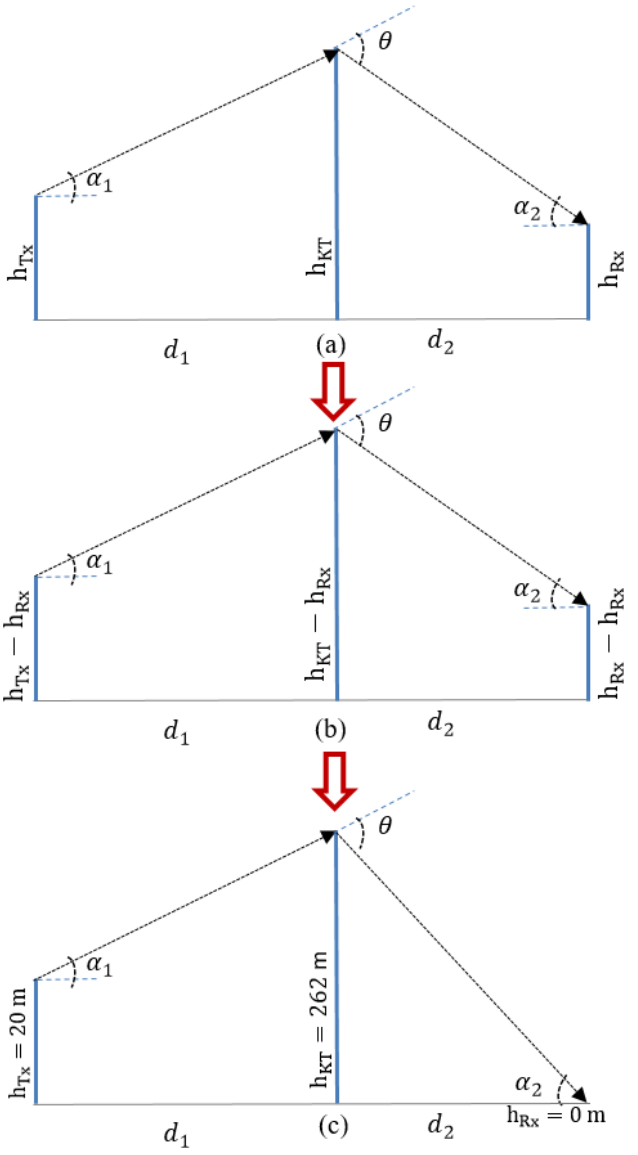

FIGURE 6. The approximation geometry method steps (a) to (c) of the proposed KED model shown in Fig. 3: (a) converting Fig. 3 into a geometrical shape, (b) applying approximation by subtraction h_{RX} from each height, and (c) is the final geometrical values for diffraction element heights. Where the original heights are as follows: $h_{KT} = 302$ m, $h_{TX} = 60$ m, and $h_{RX} = 40$ m.

in that order). It is worth to mention that the specific attenuation or ERA practically depends on the raindrop diameters, falling speed of raindrops, and the number of dominant diameter drops [42].

In addition, the distance factor, r, is computed according to the formula (11), in which the parameter d_0 is the effective path length, in km. It can be computed as:

$$d_0 = 35e^{-0.015 \cdot RR_{0.01}} \tag{10}$$

$$r = \frac{1}{1 + \frac{d}{d_0}} \tag{11}$$

For a case of $RR_{0.01}$ is greater than 100 mm/h, we use 100 mm/h instead of $RR_{0.01}$.

In addition to rain attenuation, the KED loss, L_{ked}, has been included in Eq. (4) since the PPT system functions under the effect of high buildings that have sharp- or knife-edges. When an object makes the signal diffracted, the diffracted electromagnetic energy on the shadow area behind the object (at the receiver) reduces the arrival energy to the receiver. In the diffraction phenomenon, the electromagnetic waves bend at the edge of a blockage, and it can be explained by Huygen's principle [43] which declares that each individual point on a wavefront works as a source of a secondary ''wavelet'' and all resultants ''wavelets'' are added so as to provide another wavefront in the direction of propagation, and so on. If the object blocks a portion of the wavefront, the near wavelets to the blockage undergo counterbalanced, and thus radiation does not occur in directions of the plane wave [44]. Due to the plane wave incident on the KED point, the shadow area can be divided into three shadow regions based on the position of the KED point either above, below, or directly on the LOS between the Tx and Rx [44]. In our proposed scenario, based on [38] the Tx antenna side is higher than the Rx antenna, i.e., the KED point is above the LOS between the transmitter and receiver. Besides, the KED situation in Fig. 3 can be appoximated in a similar geometry way to that exemplified in Fig. 6 with the purpose of calculating the Fresnel-Kirchoff diffraction (FKD) parameter which is employed to

produce the KED loss. Consequently, it is suitable to use the succeeding mathematical expression for obtaining the FKD parameter before the final step to obtain the diffraction loss, L_{ked} [19], [43]:

$$\alpha_1 = \tan^{-1}\left(\frac{(h_{KT} - h_{RX}) - (h_{TX} - h_{RX})}{d_1}\right) = \tan^{-1}\left(\frac{h_{KT} - h_{TX}}{d_1}\right) \quad (12)$$

$$\alpha_2 = \tan^{-1}\left(\frac{(h_{KT} - h_{RX}) - (h_{RX} - h_{RX})}{d_2}\right) = \tan^{-1}\left(\frac{h_{KT} - h_{RX}}{d_2}\right) \quad (13)$$

$$\theta = \alpha_1 + \alpha_2 \quad (14)$$

$$v = \theta\sqrt{\frac{2\,(d_1 d_2)}{\lambda\,(d_1 + d_2)}} \quad (15)$$

where d_1 is the Tx-KT separation distance between the transmitter, Tx, and the KT, and d_2 is the KT-Rx separation distance as shown in Figs. 3 and 6, while h_{KT}, h_{TX}, and h_{RX} denote heights of the KED difrraction (KT), the Tx, and the Rx, correspondingly. Additionally, α_1 and α_2 are the angles, in rad, between the knife-edge of the tower (KT) and each antenna of the Tx and Rx end when seen from the other end, while θ is the angle of KED in rad [17], [19], [43]. As illustrated in Fig. 7, All the abovementioned parameters are defined. Consistent with the proposed scenario, the geometry of Fresnel diffraction has been implemented as displayed in Fig. 7 in order to simulate the PPT communication link early displayed in Fig. 3. All figures (Figs. 3 and 7) indicate that KED height is positive, hence α and v are positive also. Moreover, by referring to Table 2 and the specification of the PPT system, the heights of the Tx and Rx are smaller than the Tx-Rx separation distance. As a result, we can claim that the Rx is located in the shadow area behind the KT tower. With the understanding that the Rx is situated in the diffraction zone or what we called ''shadowed region'', the strength of the electrical E- field at the receiver is the addition of all fields, as vectors, caused by secondary Huygen's wavelets in the plane above the KED at the diffraction twoer [17]. The E-field due to the diffracted path, E_d, can be expressed by the diffraction integral:

$$E_d = F(v) = E_0\frac{(1+j)}{2}\int_v^{\infty}\exp^{(\frac{-j\pi t^2}{2})}dt \quad (16)$$

where $F(v)$ is the complex Fresnel integral, E_0 is the E-field at the Rx considering only free space loss, and v is the FKD parameter which is a dimensionless factor and often used to reduce the symbol representation in Fresnel zone analyses. Compared to the free space electric field, the diffraction loss caused by KED is expressed as:

$$L_{ked} = 20\,log\ |F(v)| \quad (17)$$

Practically, however, the diffraction loss can be numerically approximated [45] mainly as a function of the FKD parameter which can be computed as follows.

$$L_{ked} = \begin{cases} 0 & v \le -1 \\ 20\log(0.5 - 0.62v) & -1 \le v \le 0 \\ 20\log\left(0.5e^{-0.95v}\right) & 0 \le v \le 1 \\ 20\log(0.4 - (0.1184 - (0.38 - 0.1v)^2)^{0.5}) & 1 \le v \le 2.4 \\ 20\log\left(\frac{0.225}{v}\right) & v \ge 2.4 \end{cases} \quad (18)$$

III. PPT SYSTEM PARAMETERS AND SCENARIOS

The key Tx and Rx parameters of the proposed PPT system link are depicted in Fig. 7 and the parameter values are also tabulated in Table 2. Various millimeter-wave spectrum bands allocated for 5G communication systems (such as Ka and mmWave bands) have been employed for achieving the main purpose of this study. Receiver sensitivity has been assumed for all frequency bands [17], [46], [47] to be −103 dBm. In addition, some parameters of the Tx and Rx have been taken into account from LOS measurements that have been carried out on 5G carrier links [48]–[51].

The assumed PPT (KAFD-PSS) system scenarios are as follows: (a) Scenario 1 illustrates the PPT link operating at a carrier frequency of 28 GHz, the Tx and Rx use high antenna gain, and −103 dBm as a receiver sensitivity. This link experiences rain attenuation and KED impact by reason of existence of the diffraction object between KAFD and PSS ends; (b) Scenario 2 shows a link functions also at a Ka frequency carrier but here it is 38 GHz and has the same Tx and Rx gains as scenario 1. Scenario 1 is with higher urban and statistical losses compared to scenario 2; (c) Scenario 3 examines the KAFD-PSS system link statues at a carrier frequency of 60 GHz but the Tx and Rx have antennas with higher gain and the transmitted power is also higher than that of the previous two scenarios. This distinguished frequency (60 GHz) is significantly affected by very high atmospheric absorption [52]. This may cause the transmitted power to be considerably affected by huge attenuation [53]. (d) Scenario 4 shows one of the E-band frequency of 73 GHz. This scenario has lower Tx antenna gain compared to 60 GHz, but it has approximately the same transmitted power and receiver antenna gain; (e) Scenario 5 represents the PPT link that operates at 100 GHz and approximately employs the same parameters as scenario 4 except it is with a higher directive transmitted antenna gain. Obviously, all links are assumed to function with aid of directional antennas; for the transmitters, a parabolic antenna with 0.6 m diameter has been employed while for the receiver side, horn antennas are suggested [54], [55].

As can be seen from [53, Fig. 2], the frequency 60 GHz is the only frequency among the first hundred gigahertz of the frequency spectrum which is influenced by a very high atmospheric absorption. It is found that 98% of the transmitted energy in the 60 GHz is absorbed by atmospheric oxygen. Several previous research works indicated that some carrier frequencies, in addition to 60 GHz, undergo various

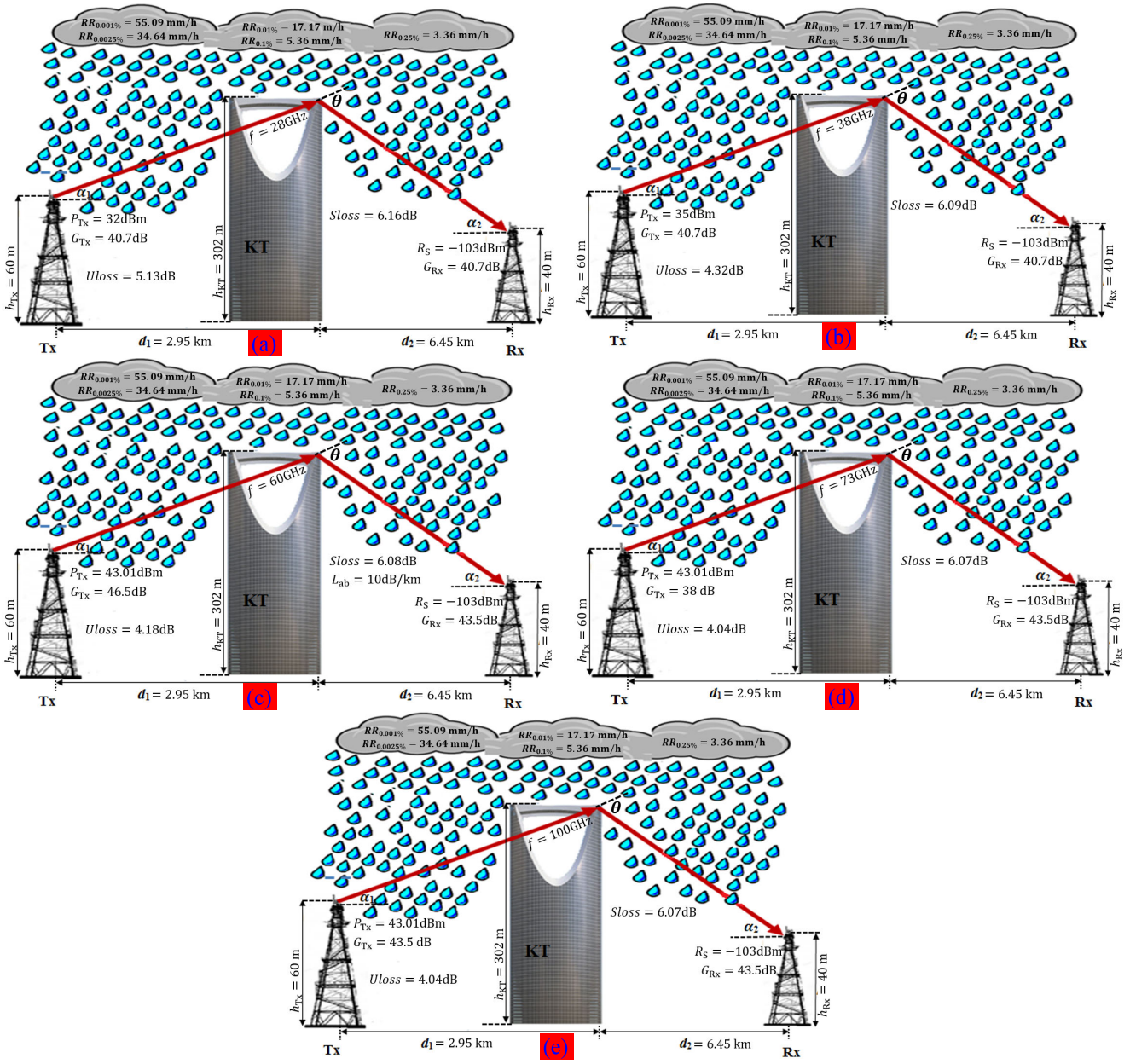

FIGURE 7. The proposed PPT scenarios and specification of the links under investigation for: (a) scenario 1, (b) scenario 2, (c) scenario 3, (d) scenario 4, and (e) scenario 5 which are pronounced in Table 2. The values of angles (θ, α_1, and α_2) are adjustable based on the distance d_1 and d_2, the heights of Tx, Rx and the diffraction object KT. The rain rates are tabulated in Table 3.

levels of atmospheric absorption loss due to oxygen and water molecules. This phenomenon creates an extra loss per traveled distance which is added to the total link power budget. The other frequency bands that affected by atmospheric absorption include 183 GHz, 325 GHz, and 380 GHz [53], [56], [57]. These studies clarified that, at 60 GHz, the atmospheric absorption can cause fading of roughly 10 dB/km.

With the purpose of estimation of environment channel parameters for the designed situations in Fig. 7, Nautel's RF toolkit is utilized to obtain a number of the system parameters. These include urban and statistical losses, antenna heights, and the locations of the transmitter and the receiver. The urban loss occurs due to clutter with urban-type that appears within the Fresnel zone [17], while, the statistical loss is some extra loss comes to the picture because of effect of the terrains which are counted in the link budget [57]. Nautel's toolkit uses a digitized database for terrain called shuttle radar terrain mapping (SRTM) offered by the America National Aeronautics and Space Administration (NASA).

The extracted parameters from the abovementioned toolkit have been inserted into a Matlab code used to simulate the assumed model. Moreover, the collected measurement data of the rain rates in Riyadh city have been converted into mm/h which in turn included in the ITU-R model to obtain the

TABLE 3. Rain rates for different year percentages and scenarios using horizontal polarization situation.

Year Percentage (%)	Rain rate (mm/h)	ERA H-Pol (dB/km) For 28GHz	Rain Attenuation, H-Pol (dB)				
			Scen. 1	Scen. 2	Scen. 3	Scen. 4	Scen. 5
0.001	55.09	9.934	72.84	100.54	135.83	143.72	154.02
0.0025	34.64	6.340	46.48	66.79	95.22	102.21	112.27
0.01	17.17	3.214	23.57	35.97	55.64	61.04	69.59
0.1	5.36	1.042	7.637	12.89	22.82	25.96	31.47
0.25	3.36	0.663	4.860	08.54	15.96	18.42	22.89

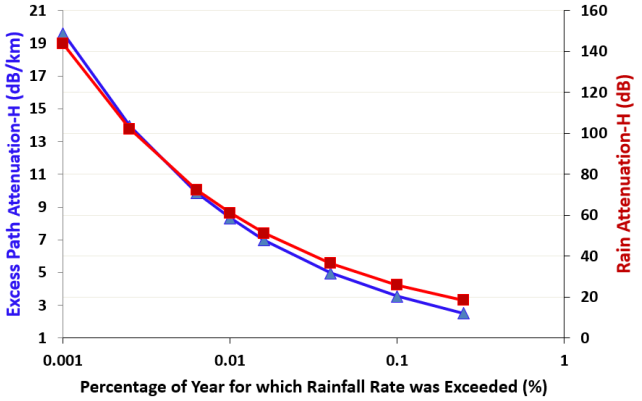

FIGURE 8. Excess rain rate (dB/km) and corresponding rain attenuation (dB) for horizontal polarization at 73 GHz for the PSS-KAFD path link in Riyadh, as an example.

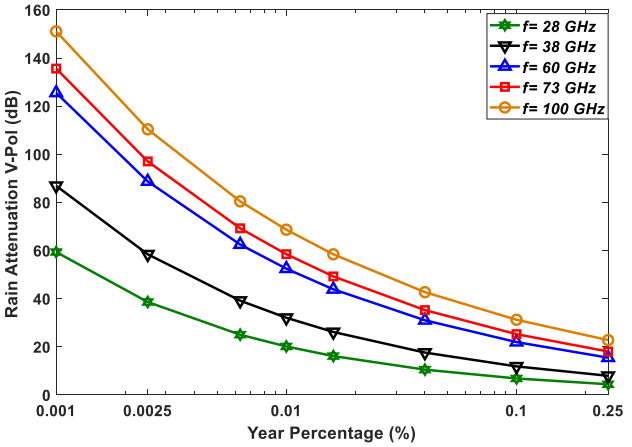

FIGURE 9. Rain attenuation (dB) for vertical polarization in Riyadh using ITU-R model.

excess rain attenuation (ERA) in dB/km due to rain, as shown in Fig. 8. Then, total rain attenuation due to the entire path is calculated for the worst case which is resultants from the horizontally polarized type. Various rain rate exceedance has been considered in order to determine the amount of fading that can be occurred in a percentage of the year for which rainfall was exceeded. Rain rate exceedance of 0.001%, 0.0025%, 0.01%, 0.1% and 0.25% have been selected to study effect of maximum rain rate attenuation (0.001% and 0.0025%), medium attenuation (0.01%), and low attenuation (0.1% and 0.25%). Commonly, a rainfall rate value of 0.01% exceedance (it approximately equals to only 52.56 minutes per year which means that a link is unavailable for 0.01% of the year), and it means also that it is available for 99.99% of the time (99.99% rain availability). The value of 0.01% exceedance is of key interest for the sustainability of satellite and terrestrial communication links. This important parameter is frequently referred to as RR0.01 and is measured in mm/h.

IV. RESULTS AND DISCUSSION

In this section, we are going to show and analyze the obtained results of this research work. The signal strength level at the receiver under the worst case is analyzed and discussed for various yearly rain rates exceedance as shown in Table 3. This table shows measured and collected rain rate data for each year percentage exceedance scenario in mm/h, its corresponding excess rain attenuation (ERA) or specific attenuation in dB/km for the 28 GHz worst case which is horizontally polarized (as an example), and then the total path link attenuation for the proposed PPT wireless link. In Table 3, it can be noticed that the rain rates are arranged in the descending order based on the year percentage of rain exceedance; such that the first row rain rate of 55.09 mm/h can cause the maximum excess rain attenuation (ERA) (or specific attenuation) of 9.934 dB/km at 28 GHz (in horizontal polarization) for example, and this value leads to an attenuation of 72.84, 100.54, 135.83, 143.72, and 154.02 dB for scenarios 1 to scenario 5, respectively. In addition, horizontally polarized rain attenuation levels at 73 GHz with its corresponding ERA levels have been depicted in Fig. 8 to show the two terms relation. Moreover, according to Figs. 9 and 10, the observed difference between rainfall attenuation using vertical polarization (Fig. 9) and horizontal polarization (Fig. 10), which is also in consistency with previous studies such as [60], [61], reveals that the horizontal polarization is the worst case and it is the polarization considered in this paper. Moreover, Table 3 and Fig. 10 demonstrate that the minimum attenuation occurs for 0.25% exceedance which causes a horizontally polarized ERA of 0.663 dB/km and creates attenuation of 4.86, 8.54, 15.96, 18.42, and 22.89 dB for scenario 1 to scenario 5, correspondingly.

The losses due to KED [62] have been computed such that the Tx is sited at changed locations, i.e., the distance d_1 (in Fig. 7 (a-e)) is adjustable (0.2-2.95 km) while the distance d_2 is reserved stationary ($d_2 = 6.45$ km). Consequently, the KED loss for a path length less than 2.95 km (there are no materials/ objects block the transmit signal) will be zero due to the fact that diffraction conditions are not achieved according to Eqs. (12)-(18). In this syntax, for scenario 1, the diffraction loss is nearly 56.74 dB as a maximum value when the distance d_1 is minimum (when the Tx is 0.2 km away from the diffraction object (KT)), whereas the minimum loss is 49.4 dB (the transmitter is 2.95 km ahead of the diffraction object).

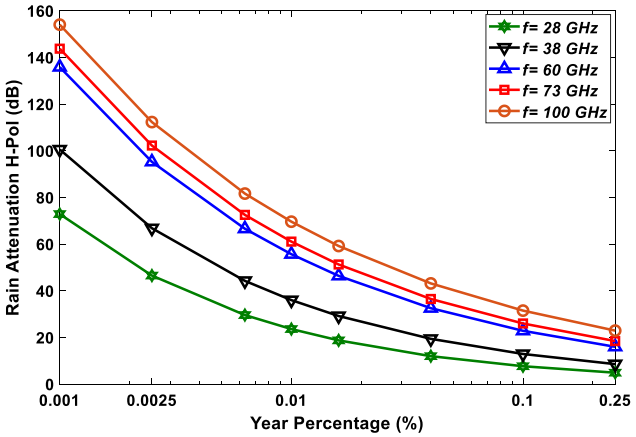

FIGURE 10. Rain attenuation (dB) for horizontal polarization in Riyadh using ITU-R model.

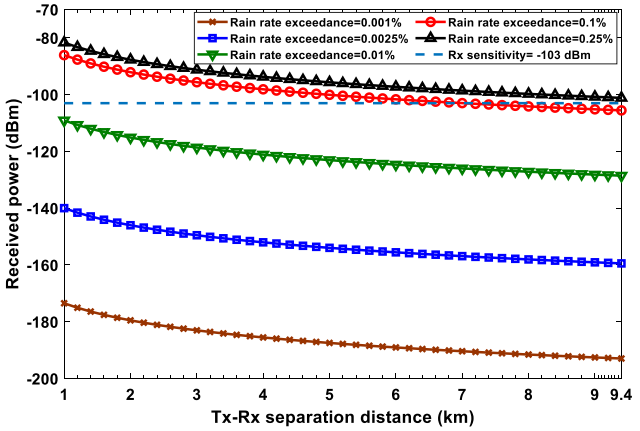

FIGURE 12. The Tx-Rx separation distance against the received power for scenario 2 for different rain rate exceedance cases, where $h_t = 60$ m, $h_r = 40$ m, and $f = 38$ GHz.

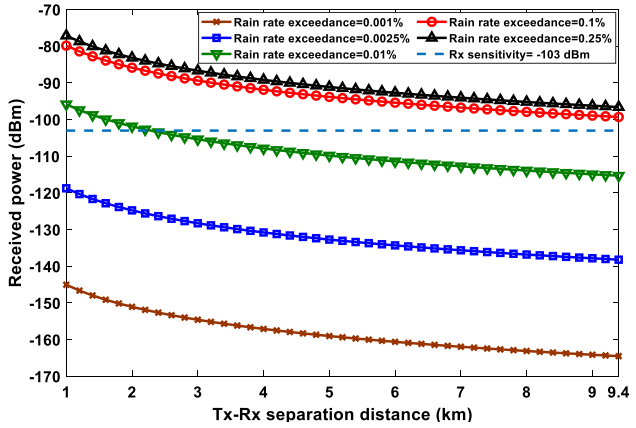

FIGURE 11. The Tx-Rx separation distance against the received power for scenario 1 for different rain rate exceedance cases, where $h_t = 60$ m, $h_r = 40$ m, and $f = 28$ GHz. The five rain rates exceedance cases in the figure correspond to that cases in Tables 2 and 3.

In Fig. 11, the received signal power versus the Tx-Rx separation distance for scenario 1 is clarified for the abovementioned five rain rate readings at 28 GHz. It is apparent from Fig. 11 that the signal strength level declines from −77.14 to −164.5 dBm as the Tx-Rx separation path increases from 1 km to 9.4 km for all rainfall rates. It is clear that if the signal experiences rain rates of 5.36 mm/h (0.25% rain rate exceedance) or 3.36 mm/h (0.1% rain rate exceedance) its level at the antenna receiver will be higher than the receiver sensitivity by 6.4 and 3.6 dB, respectively. While, the received power level under rain rate of 17.17 mm/h (0.01% rain rate exceedance would not be able to go more than 2.2 km, i.e., it is far away from the receiver due to the fact that the signal strength level will be weak and less than −115 dBm when it reaches the receiver which means that there is a fade margin of roughly −12 dB with respect to receiver sensitivity. In addition, the other two cases which are affected by rain rates of 34.64 and 55.09 mm/h for link availability of 99.9975% and 99.999% of the time, the signal suffers from very high attenuation of roughly 46.5 and 73 dB due to rain, in that order, and 49.4 dB due to KED effect that influences all the cases.

The results using 38 GHz represented by scenario 2 are shown in Fig. 12. It can be realized that the PPT system only operates under link availability of 99.75% of the time which affected by a rain rate of 3.36 mm/h. In which, the minimum received signal power is −101.2 dBm and this value is still above the sensitivity of the receiver. Whereas, the receiver location must be at a distance not longer than 7 km from the transmitter to be able to detect the transmit power in case of the rain rate becomes more intensive (5.36 mm/h). This is because that the transmit signal strength at the KAFD station will be under the receiver sensitivity by 2.6 dB which is not acceptable to detect the signal. As shown in Fig. 12, the system will not function if the rain intensity becomes high for 0.01%, 0.0025%, or 0.001% exceedance where the receiver can not detect signals with strength levels of −128.6, −159.5, or −193 dBm, correspondingly, because of the large attenuation of rainfall and diffraction. These two phenomena (rainfall and diffraction) cause fading of approximately 36, 67, and 101 dB for the 0.01%, 0.0025%, or 0.001% rain exceedance, respectively.

For scenario 3 which employs the frequency 60 GHz, not surprisingly that the performance was highly disappointing as shown in Fig. 13. This figure illustrates that scenario 3 is totally not able to work under rain even if it is with low intensity and also under diffraction due to the fact that it causes NLOS propagation condition which is not proper circumstances for a frequency experiences 10 dB/km loss due to atmospheric absorption. This high attenuation loss comes from oxygen absorption which can severely limit range, but it has a benefit that it can also eliminate interference between the same frequency terminals. This effective factor ''atmospheric absorption'' can make a total atmospheric absorption link loss of 94 dB attenuation for our proposed PPT link which looks a dominant factor in this band especially if the

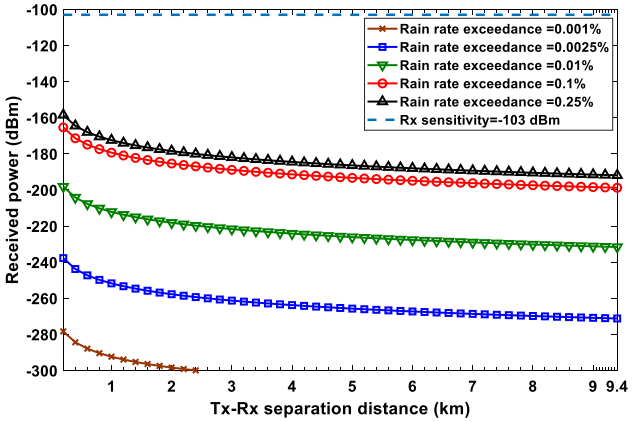

FIGURE 13. The Tx-Rx separation distance against the received power for scenario 3 for different rain rate exceedance cases, where $h_t = 60$ m, $h_r = 40$ m, and $f = 60$ GHz.

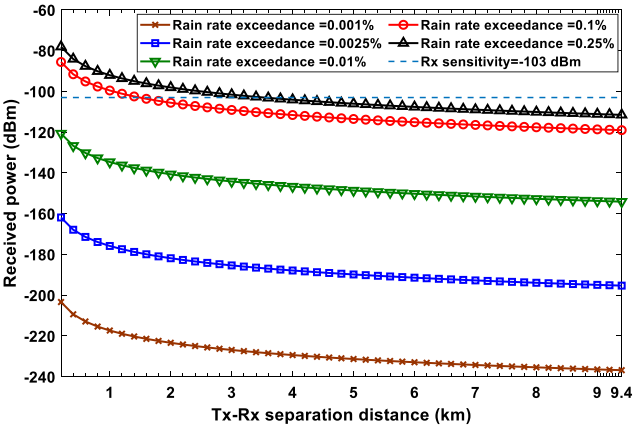

FIGURE 14. The Tx-Rx separation distance against the received power for scenario 4 for different rain rate exceedance cases, where $h_t = 60$ m, $h_r = 40$ m, and $f = 73$ GHz.

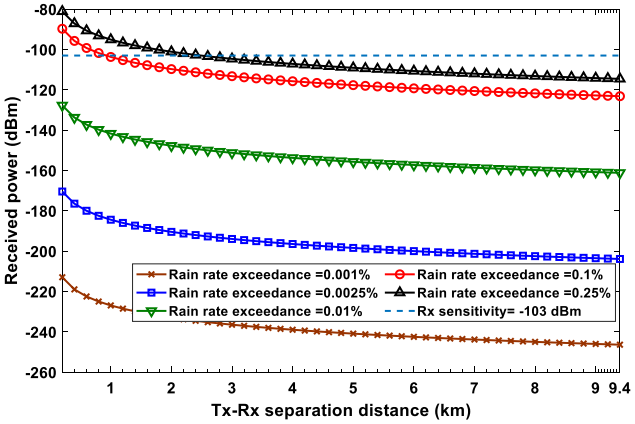

FIGURE 15. The Tx-Rx separation distance against the received power for scenario 5 for different rain rate exceedance cases, where $h_t = 60$ m, $h_r = 40$ m, and $f = 100$GHz.

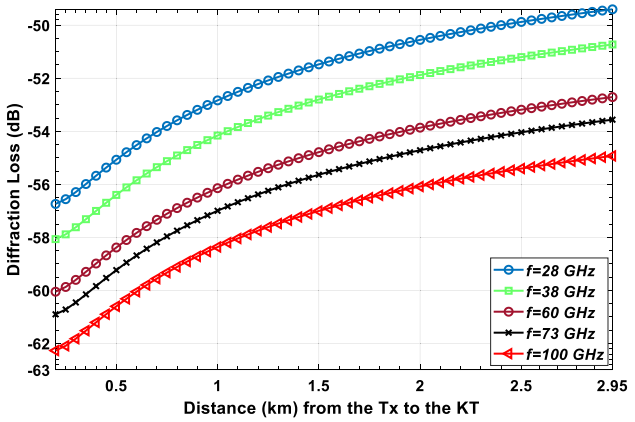

FIGURE 16. The resultant KED losses against the Tx–KT separation distance which corresponds to diffraction loss of the Tx-Rx link distance of approximately 2.95 to 9.4 km where the diffraction loss is considered within this path.

Tx-Rx separation distance is large. Significantly, the power level at the KAFD receiver is hugely out of receiver capability to detect the transmit power which has a strength level of −192 dBm in the best weather conditions and declines to less than 300 dBm. Consequently, it can be said that this situation for 60 GHz link makes scenario 3 maybe not proper for outdoor communication, it seems very likely to be more appropriate for indoor communication instead.

Figs. 14 and 15 display scenarios 4 and 5, respectively. It seems that these two scenarios are almost the same where the two minimum rain rate intensities of 3.36 and 5.36 mm/h have less effect on the signal strength than the higher ones. That is, the power level at 9.4 km for 73 GHz and 100 GHz has been dropped to nearly −111.5 dBm and −115 dBm for the lowest rain rate and around −237 dBm and −246 dBm for the highest rain rate, respectively. These two rain intensities in addition to KED influence make the maximum distance that the receiver is able to pick up the signal only at 3.6 km and 1.5 km for 73 GHz, and at 2.5 km and 1 km for 100 GHz, respectively, which are less than our link range. Whereas, after these separation distances the signal levels will be impractical and can not appropriately be received since the receiver sensitivity is very much higher than that presented in Figs. 14 and 15 of the received power levels that probably fall within noise power levels. Categorically, the large attenuation losses in case of low rain rates (3.36 and 5.36 mm/h) are essentially supported by the path loss which is roughly 149 dB using 73 GHz and 152 dB using 100 GHz, the rainfall approximately of 18.4 dB and 26 dB using 73 GHz, and 23 dB and 31.5 dB using 100 GHz for rain rate exceedance of 0.25% and 0.1%, in that order, and then diffraction mechanism that contributes by 54 dB and 55 dB for scenarios 4 and 5 respectively, as shown in Fig. 16. Therefore, at low rain rate exceedance (0.25% and 0.1%) the minimum recommended receiver sensitivity should not be less than −123 dBm for all scenarios except scenario 3. However, in case of a high rain rate, the potential outage may be probably occurring due to high rain attenuation as a dominant attenuation factor followed by the free space path loss and then the effect of KED diffraction stands thirdly.

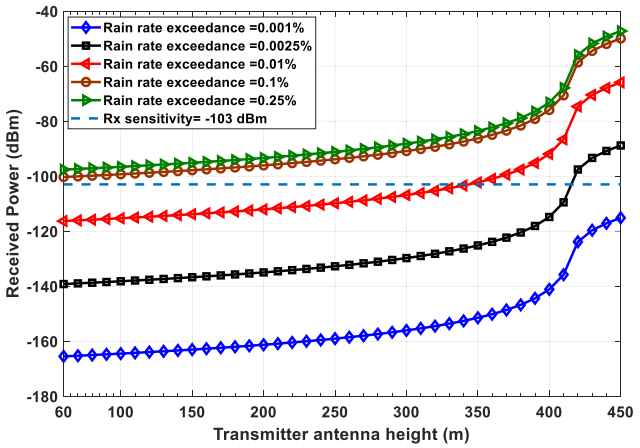

FIGURE 17. Variation of the transmitter antenna height versus the power received for scenario 1 ($f = 28$ GHz), $h_r = 40$ m, the Tx-Rx distance = 9.4 km.

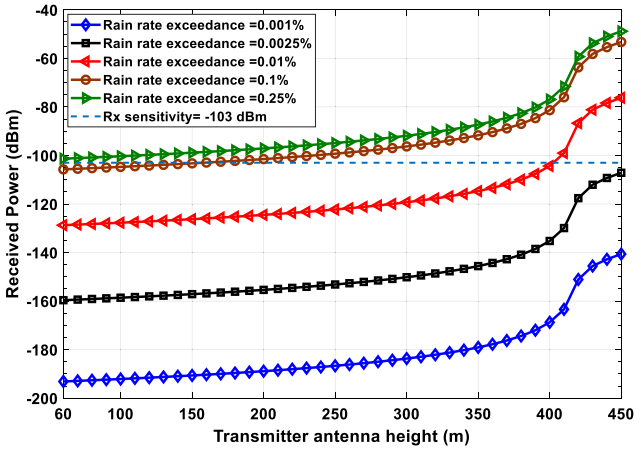

FIGURE 18. Variation of the transmitter antenna height versus the power received for scenario 2 ($f = 38$ GHz), $h_r = 40$ m, the link distance = 9.4 km.

The aforementioned findings indicate that the signal strength level will inappropriately be detected in most circumstances and situations. In view of that, it is proposed to raise the transmitter antenna height from 60 m to 450 m using a higher mast for all assumed scenarios. The findings of employing higher antenna mast are illustrated in Figs. 17-21. In Fig. 17 (scenario 1), we observed that in the case of low rain rates (3.36 and 5.36 mm/h) with normal antenna heights ($h_t = 60$ m and $h_r = 40$m) the PPT link operates with acceptable performance and no need to rise the antenna height. While, in case of rain rate exceedance of 0.01% and 0.0025%, minimum antenna heights of 342 m and 415 m are necessary for scenario 1 to receive sufficient signal power from the Tx which is sited at 2.95 km south of the KT tower. On the other hand, the signal would not be received for any of the proposed antenna heights when the rain rate is more intensive such as 0.001% exceedance, in which a fade margin of 12 dB will be essential to detect the signal at the KAFD station.

In Fig. 18, employing 38 GHz in scenario 2 imposes using an antenna with a higher mast of 160 m for rain rate exceedance of 0.1% whereas the case of 0.25% still can work with normal antenna height. Additionally, an antenna mast with a height of 403 m is compulsory to receive a signal from the PSS station (Tx). However, for the most intense two rain rates, the signal may not be detected within the proposed maximum antenna height (450 m) due to the fact that maximum attenuation at those rain rates exists which causes very high losses and negatively contributes to the power link budget. That is, using an antenna height of 450 m can not fulfill the minimum power requirement at the receiver, thus the power margin is -4 dB and -38 dB under link availability of 99.9957% and 99.999%, correspondingly. In contrast, all proposed antenna heights are not enough for all rain rate intensities using 60 GHz as shown in Fig. 19. In this figure, we can clearly notice that received power at the receiver for all the five cases is highly less than the receiver sensitivity. This means that antenna lifting is not a proper solution to efficiently keep the PPT system at 60 GHz operating. On the other hand, for Scenarios 4 and 5 shown in Figs. 20 and 21, an antenna height of 283 m, 364 m, and 429 m using an operation frequency of 73 GHz, and 335 m, 386 m, and 444 m using 100 GHz must be achieved for the PPT links which experience rain intensities of 3.36, 5.36, and 17.17 mm/h, respectively, so as to make the link under continuous operating. Exceptionally, the PPT link will not function if heavy precipitation rates (34.64 and 55.09 mm/h) fall on this system, in which the power received is not higher enough to be detected. From Fig. 22 that represents the effect of antenna heights for scenario 1 and rain rate exceedance of 0.0025%, as an example, it can be seen that the variable antenna height for the proposed scenario behaves as a cube root function where the height of 420 m represents the inflection point at which the cube root function changes its sign, where the height of transmit antenna is assumed to be variable from 100 m to 800 m for the purpose of showing that the relationship between the received power and antenna height approximately follows a cube root function.

Furthermore, so as to distinguish between the influence of rain attenuation and KED mechanism separately we demonstrate to simulate the PPT link for all scenarios as shown in Figs. 23-27. In this simulation we considered normal antenna height ($h_t = 60$ m and $h_r = 40$ m) and divided the PPT link situations to be under the influence of four cases: (i) with no rain and no diffraction, (ii) with both rain and diffraction, (iii) with rain and no diffraction, and (iv) with no rain and with diffraction. It is worth to note that in case of that the link undergoes rain effect, the rain rate exceedance of 0.01% has been assumed as an average case. For case (i) in scenario 1 represented in Fig. 23, we can observe that system will operate in a physically relaxed mode under clear-sky (no rain) and also under no a diffraction object can block the transmitted signal. So this system situation is under LOS condition and the main effect is the free space propagation

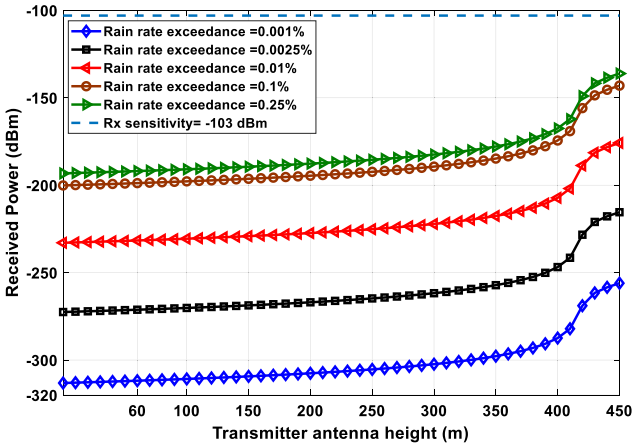

FIGURE 19. Variation of the transmitter antenna height versus the power received for scenario 3 (f = 60 GHz), h_r = 40 m, the Tx-Rx distance = 9.4 km.

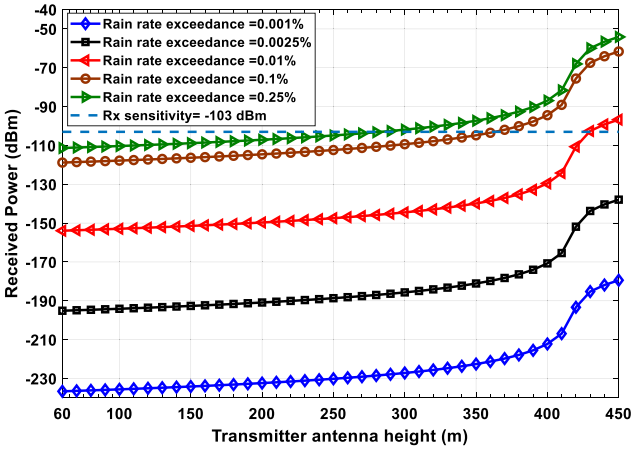

FIGURE 20. Variation of the transmitter antenna height versus the power received for scenario 4 (f = 73 GHz), h_r = 40 m, the Tx-Rx distance = 9.4 km.

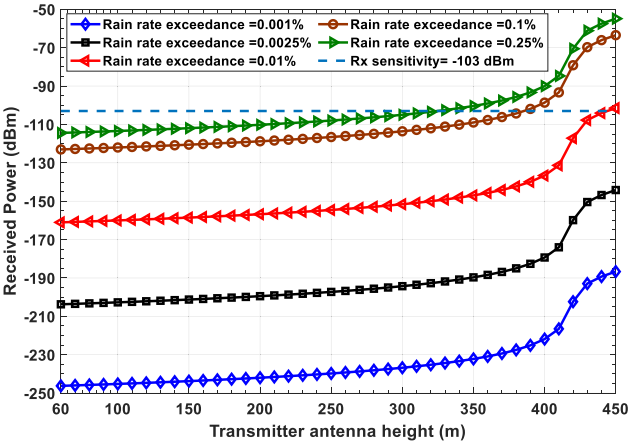

FIGURE 21. Variation of the transmitter antenna height versus the power received for scenario 5 (f = 100 GHz), h_r = 40 m, the Tx-Rx distance = 9.4 km.

loss. Thus the signal strength level is always very high and much higher than the receiver sensitivity, where the signal power at the receiver is about −40 dBm which provides high

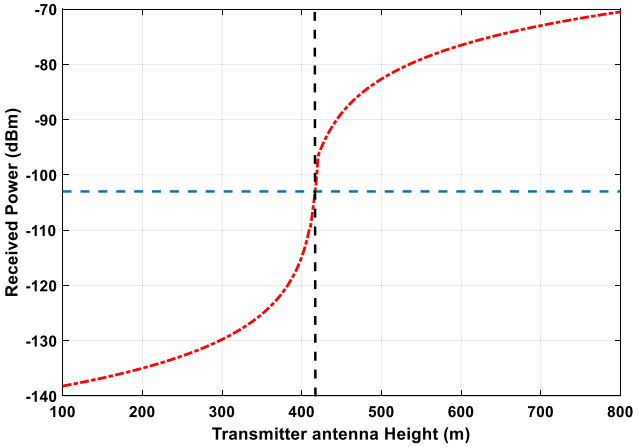

FIGURE 22. The power received versus antenna height variation for scenario 1 (f = 28 GHz), h_r = 40 m, the Tx-Rx link distance = 9.4 km. and rain rate exceedance of 0.0025% to show that this relation behaves as a cube root function (This curve is the same as the second curve from the bottom with a square mark and black color as shown in Fig. 17).

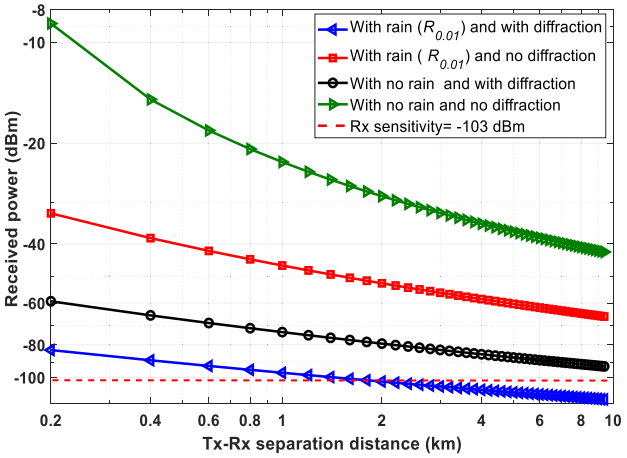

FIGURE 23. The received power versus the Tx-Rx separation distance for various conditions with and with no rain (clear-sky) conditions and with and with no diffraction mechanism, f = 28 GHz, rain rate = 17.17 mm/h, ERA = 3.21 dB/km, and rain attenuation ($R_{0.01}$) = 23.6 dB.

performance. For the second case where the system link is under both rain and KED diffraction, the system suffers from three main effects: rain, diffraction, and path loss. In this case, the system experiences a NLOS environment due to diffraction object (the KT building), therefore, this is the worst case for this link, and we can see from Fig. 23 that the maximum distance is around 2.1 km which is before the diffraction location. This means that system can not operate under the defined specifications. On the other hand, for the two cases (iii) and (iv) we can observe that the effect of attenuation created by the diffraction mechanism is higher than that of the rainfall event. That is, the power received at the KAFD receiver station is about −66 dBm and −93 dBm for case (iii) and (iv) respectively. This is due to the fact that diffraction contributes by attenuation of 50.5 dB for the proposed path, whereas the maximum attenuation for the rain

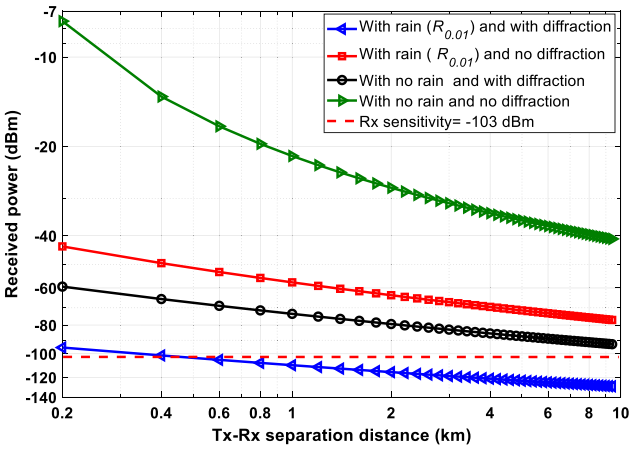

FIGURE 24. The received power versus the Tx-Rx separation distance for various conditions with and with no rain (clear-sky) conditions and with and with no diffraction mechanism, (f = 38 GHz) and rain rate = 17.17 mm/h, ERA = 4.9 dB/km, and $R_{0.01}$ = 35.97 dB.

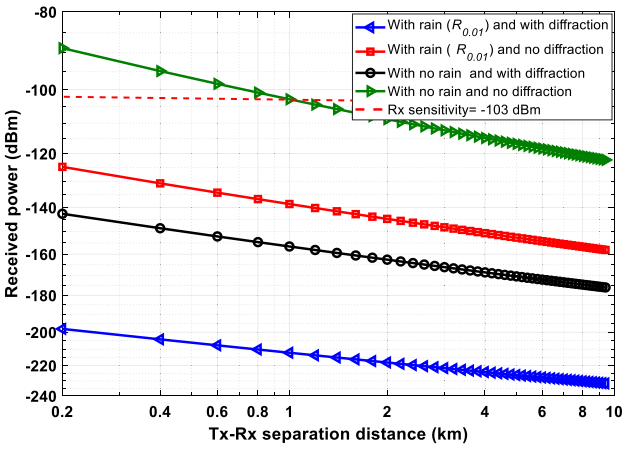

FIGURE 25. The received power versus the Tx-Rx separation distance for various conditions with and with no rain (clear-sky) conditions and with and with no diffraction mechanism, (f = 60 GHz) and rain rate = 17.17 mm/h, ERA = 7.58 dB/km, and $R_{0.01}$ = 55.6 dB.

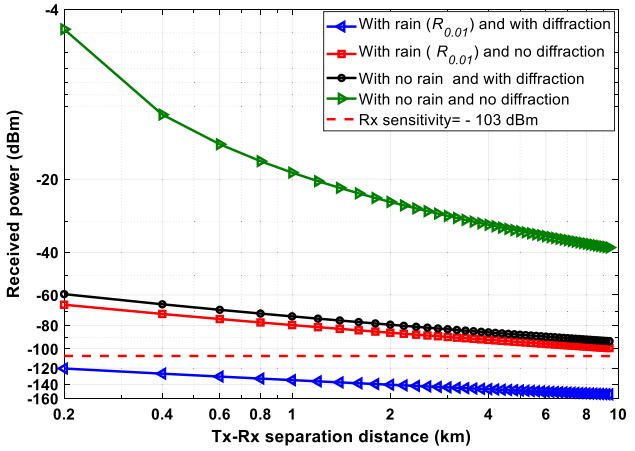

FIGURE 26. The received power versus the Tx-Rx separation distance for various conditions with and with no rain (clear-sky) conditions and with and with no diffraction mechanism, (f = 73 GHz) and rain rate = 17.17 mm/h, ERA = 8.3 dB/km, and $R_{0.01}$ = 61 dB.

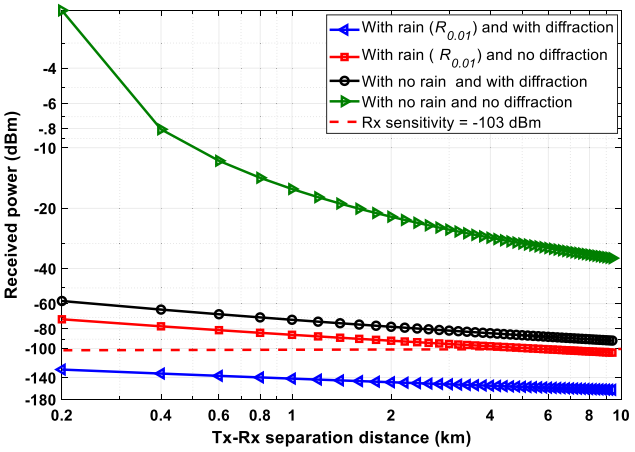

FIGURE 27. The received power versus the Tx-Rx separation distance for various conditions with and with no rain (clear-sky) conditions and with and with no diffraction mechanism, (f = 100 GHz) and rain rate = 17.17 mm/h, ERA = 9.5 dB/km, and $R_{0.01}$ = 69.6 dB.

rate exceedance of 0.01% is approximately 24 dB. However, the PSS-KAFD link is still able to operate under these two cases. It means that the scenario 1 system link can properly operate under the influence of one of the two phenomena (either rain or diffraction), not both. For scenario 2 system link displayed in Fig. 24, it looks similar to scenario 1 except for the values resultant from the simulation for the four cases. The signal power at the receiver is about −41 dBm for the case of no rain and no diffraction. In addition, for the second case (ii) the maximum distance is about 0.5 km which also out the link range. This means that the system can not work under both rain and diffraction effects. Nevertheless, for the two cases (iii) and (iv) in scenario 2 we can observe that the fade margin between the two cases becomes smaller (compared to that in scenario 1) due to increasing the effect of rain attenuation at the frequency operation 38 GHz. Then again, for both two cases (iii and iv) the system is able to peacefully work, where one phenomenon is there while the other is absent. However, the diffraction effect still has superiority over the rain attenuation effect for the same reason abovementioned.

Moreover, as illustrated in Fig. 25, scenario 3 experiences the highest attenuation, and this is because of the existence of the additional loss represented by the atmospheric absorption at the operation frequency of 60 GHz even in clear-sky case (i). In this case, 1 km is the maximum distance in which the signal stays always above the sensitivity threshold for scenario 3, but it is useless for the PSS-KAFD link. Whereas the other three cases (ii, iii, and iv) in this scenario can not absolutely achieve the minimum requirement to pick up the signal, and thus the signal strength levels are always under the sensitivity threshold.

In addition, scenario 4 (73 GHz link) is illustrated in Fig. 26. In case (i), the link is under the clear-sky condition and with no diffraction circumstances, and thus the signal is

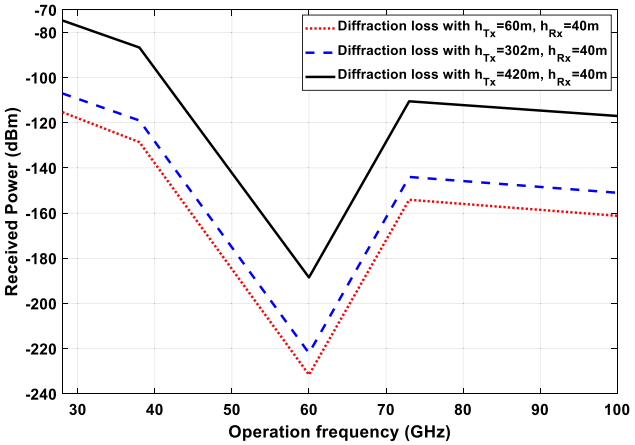

FIGURE 28. The received power at the KAFD Rx (9.4 km) versus the operation frequencies experiences rain rate of 17.17 mm/h (rain rate exceedance of 0.01%) for different transmitter antenna heights and fixed receiver antenna height.

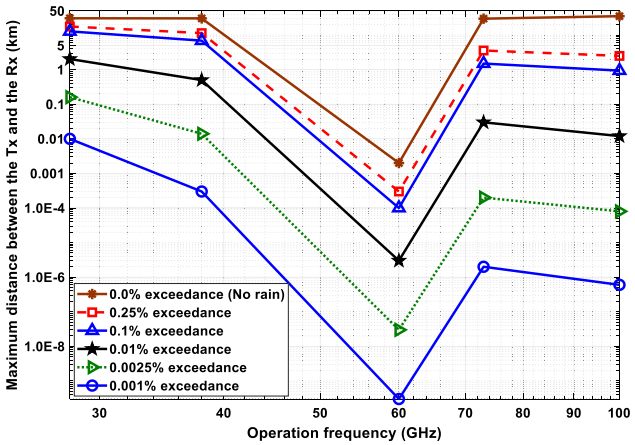

FIGURE 29. The maximum Tx-Rx distance that the power may reach versus the operation frequency based on normal antenna heights and receiver sensitivity of −103 dBm, for all scenarios (frequencies) and case (ii) with all rain rate exceedances as well as the clear-sky condition.

always higher than the threshold of the receiver. Regardless, the received power is −38.3 dBm which is higher than that of scenarios 1 and 2 although that the only dominant factor for case (i) is the path loss that is at 73 GHz (149.2 dB) greater than that of 28 GHz (140.6 dB) and 38 GHz (143.5 dB). This is because that scenario 4 (similarly scenario 5) uses particular Tx/Rx with higher power and the antenna gain of the Rx is also higher than that of scenarios 1 and 2 (see Fig. 7 and Table 2). These higher values of the transmit power and antenna gains of scenarios 4 and 5 compensate for the shortcoming in the path loss difference. As long as the path loss difference is less than the difference of the additive values of antenna gains and transmitter power the signal strength of 73 GHz and 100 GHz PPT systems is higher than that of scenario 1 as well as scenario 2 as illustrated in Figs. 26 and 27 compared to Figs. 23 and 24. Moreover, for the worst case which is the case (ii), it seems that it is difficult to obtain a good connection for the two scenarios 4 and 5. This is since the received power undergoes both very high

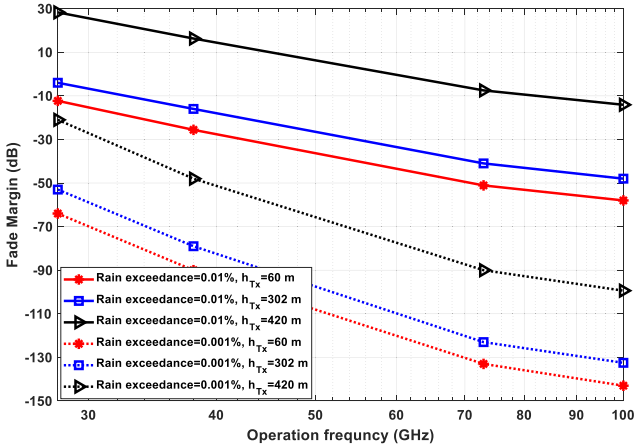

FIGURE 30. Fade margin versus the operation frequencies (28, 38, 73, and 100 GHz) for different transmitter antenna height (h_t = 60, 302, and 420 m) and for two rain rate exceedances of 0.01% and 0.001%.

rainfall attenuation and also high diffraction loss and this power is always lower than the receiver threshold, where it is approximately −154 dBm and −161 dBm for case (ii) in both scenarios 4 and 5. For the cases of (iii) and (iv), it can be noticed that there is an exchange in the effect of rainfall and diffraction on the system performance compared with that of scenarios 1, 2, and 3. i.e., it can be seen in Figs. 26 and 27 (for scenarios 4 and 5) that the influence of rainfall attenuation loss is higher than the diffraction loss compared to scenarios 1-3 in which the value of rainfall attenuation loss is lower than the diffraction loss. This is due to the fact that higher frequencies (73 and 100 GHz) experience higher attenuations which are nearly 61 dB and 70 dB for scenarios 4 and 5, respectively. On the other hand, it is worth to notice that the link related to the case (iii) in scenario 5 only works for a distance of 7.4 km since after this distance the signal power level goes below the receiver sensitivity, while this case in scenario 4 operates properly for the entire PPT system link because the transmitted signal reaches at the receiver with a level of roughly −99.3 dBm which is still above the receiver threshold (−103 dBm). However, case (iv) for scenarios 4 and 5 functions comfortably since the fade margin between the received signal and the threshold is around 10 dB and 11 dB for the two scenarios, respectively. As a summary of the results presented in Figs. 23-27, we provide (in Table 4) the cases under which system scenarios can properly work and the ones that can not properly work with the visible distance restrictions.

From Table 4 we can observe that scenarios 1, 2, 4, and 5 can properly work when either rainfall effect or diffraction effect is absent (with taking into account the restriction on the case (iii) in scenario 5). Whereas if both of them exist (case (ii)) all scenarios will not function. As expected, for case (i) which represents the clear-sky condition, all scenarios can comfortably operate except scenario 3 which its signal power serves only for less than 1 km and may be less than this distance if we take into account that this scenario uses high Tx/Rx antenna gains. Again, this means that 60 GHz

TABLE 4. The system link situations for the proposed scenarios; Where case (i) with no rain and no diffraction, case (ii) with both rain (0.01% exceedance) and diffraction, (iii) with rain (0.01% exceedance) and no diffraction, and (iv) with no rain and with diffraction. Note that √ = system operates for whole link distance with no restriction, √ [restriction]= system operates partially [for a distance after the object diffraction but less than the whole path], ×= system can not operate for the entire path link, and × [restriction]= system can not operate [except for this distance which considered not acceptable due to that it is before the diffraction object].

Scenarios	Cases			
	(i)	(ii)	(iii)	(iv)
1	√	× [less than 1.7 km]	√	√
2	√	× [less than 0.5 km]	√	√
3	× [less than 1 km]	×	×	×
4	√	×	√	√
5	√	×	√ [less than 7.4 km]	√

TABLE 5. The minimum transmitter antenna height for all scenarios in case (ii) and rain link availability of 99.99% (NA: not applicable).

Description	Scen. 1	Scen. 2	Scen. 3	Scen. 4	Scen. 5
Minimum antenna height	342 m	403 m	NA	429 m	444 m

TABLE 6. The required transmitter antenna height (m) for all scenarios and all considered rain rate exceedances, where Tx is at $d_1 = 2.95$ km from the diffraction object.

Rain rate exceedance (%)	Transmitter antenna height (m)				
	Scen. 1	Scen. 2	Scen. 3	Scen. 4	Scen. 5
0.25	60	60	NA	283	335
0.1	60	160	NA	364	386
0.01	342	403	NA	429	444
0.0025	415	NA	NA	NA	NA
0.001	NA	NA	NA	NA	NA

TABLE 7. The minimum and maximum diffraction loss in terms of the closeness or farness from the diffraction object (The KT building).

Description	Diffraction losses				
	Scen. 1	Scen. 2	Scen. 3	Scen. 4	Scen. 5
Minimum distance from KT=0.2 km	56.74	58.07	60.05	60.90	62.27
Maximum distance from KT=2.95 km	49.4	50.73	52.71	53.56	54.93

is likely to be used only for very small communications distance or indoor communication applications. The case (ii) is an undesirable situation for all scenarios when the PPT link is available for 99.99% of the time. This means that higher rain rate intensities than 0.01 % will also suffer connectionless communication. Additionally, in case of transmitter antenna height increasing has been taken into consideration for link availability of 99.99% such that 450 m is selected as a maximum height can be supplied we can see (with focusing on Figs. 17-21) that all scenarios can appropriately work provided that the restrictions on antenna height for all scenario must be achieved as shown in Table 5. In this table, it can be observed that as operating frequency increases the minimum antenna height to fulfill the system requirement increases as well. Also, from Figs. 17-21, it can summarize the required minimum antenna height for all scenarios and all rain rate exceedances as shown in Table 6. When the transmitter antenna height is not applicable (NA), this means that there is an additional gain is necessary to accomplish the receiving operation correctly. Furthermore, the KED diffraction losses have a significant contribution to the behavior of all scenarios and thus we would show the minimum and maximum diffraction loss in terms of the closeness or farness from the diffraction object (The KT building). Practically, the minimum diffraction loss occurs when the transmitter is far away from the diffraction material whereas this loss is maximum when the transmitter is very close to the diffraction material. These losses due to the diffraction mechanism are tabulated in Table 7 with help of Fig. 16. These results indicate that the diffraction influence is highly significant in the areas that are filled with tall buildings where the Tx-Rx physical path is short and definitely when the Tx/Rx is closer to the diffraction material.

In Fig. 28, we studied the effect of changing the transmitter antenna height at three elevations which are 60 m, 302 m, and 420 m, such that the first height is the normal one, the second height is the same as the diffraction height, whereas the third height is at the inflection point when diffraction loss changes its sign according to Figs. 17-22. The rain rate exceedance that has been considered for this figure is 0.01% of the time. In this figure, we can notice that the received power increases due to an increase in antenna height and a decrease in the operating frequency. Also, this figure shows that there is a huge deep signal fade at 60 GHz particularly when the transmitter height is 60 m and the power highly drops to roughly −232 dBm, while at 420 m the fading is minimum at 28 GHz where the received power equals to −74.7 dBm. Whereas the maximum received power at 302 m antenna height is about −107 dBm which is not good enough to be detectable by the receiver.

In addition, in Fig. 29, the maximum Tx-Rx separation distance that the power may reach based on a receiver sensitivity of −103 dBm against the operation frequency (scenarios) is depicted. This figure shows that there is a huge drop distance in case of 60 GHz at a link availability of 99.999% compared to clear-sky situation, such that the distance is not practically feasible and equivalent to 3×10^{-10} km (i.e., 0.3 nm), whereas this distance for the same link availability is nearly 10 m and 0.3 m at 28 GHz and 38 GHz, respectively. The maximum distance that the receiver can reach increases gradually when link availability increases while it increases when operation frequency decreases. In order to avoid misleading that may be understood from Fig. 29 especially at the clear-sky case, we may see the maximum distance is approximately the same at 28 GHz compared to 100 GHz, however, this is created by the large value of the power transmitter and antenna gain of Tx and Rx at 100 GHz compared to these parameter values for 28 GHz link (see Table 2). Again, these high values of 100 GHz system gain (approximately, the difference in the

gain between the parameters (P_t, G_t, and G_r) is 16 dB more in case of 100 GHz, which compensate the path loss difference (11.4 dB more in case of 100 GHz) between 28 GHz (140.6) and 100 GHz (152 dB). This can be understanding when we compare these two frequencies using the second curve from the top of Fig. 29, in which we can see the effect of rain on the feasible maximum distance. Definitely, the distance at 100 GHz is about 2.5 km whereas it is roughly 17.7 km at 28 GHz under the same situation. These results confirm and support the previous relationships that have been discussed in this paper.

Finally, Fig. 30 illustrates the additional fade margin or the necessary margin needed to achieve the signal power requirement due to link availability of 99.999% and 99.99% at three antenna heights of the transmitter: 60 m, 302 m, and 420 m, and for only scenarios 1, 2, 4, and 5. It can be observed that the maximum positive fade margin is 28.3 dB in scenario 1 for a link availability of 99.99% and the minimum positive fade margin is 16.3 in scenario 4 for the same availability and the same antenna height is also same (420 m). However, the maximum and minimum fade margins needed to fulfill the receiver requirements for a link availability of 99.999% and an antenna height of 60 m are 143 dB and 64 dB in scenario 5 and scenario 1 respectively. These results show that increasing the antenna height improves the fade margin specifically for scenarios 1 and 2 since this leads to acquiring a positive margin for 99.99% link availability only. This positive fade margin provides an ability to scenarios 1 and 2 to initiate reliable communication under the aforementioned conditions. Therefore, to support high reliable 5G communications, it is recommended to employ Tx/Rx with antennas have high gains; use highly sensitive receivers specifically for high rain intensity situations to overwhelmed the attenuation generated by rainfall, physical path, and diffraction; rise the antennas to a feasible and affordable height and/or may initiate communication systems within short distances particularly for higher operating frequencies.

V. CONCLUSION

This paper proposes a model can investigate the effect of rainfall and diffraction mechanism on wireless communication links. This distinctive study utilizes measured rainfall data within real urban scenarios to investigate the status of wireless system links under the rain and diffraction effects as to as analyze the PPT system link performance based on the receiver sensitivity. Several 5G carrier frequencies have been assumed to study the assumed PPT wireless links. For the proposed PPT system, the results showed that the major attenuation factor in the case of low rain intensities is the loss due to free space propagation, followed by rain attenuation, and then the loss due to diffraction mechanism. However, in case of high rainfall rates, rain attenuation comes first as a dominant factor followed by free space path loss and then diffraction loss. Additionally, the results illustrated that diffraction gain can be similarly modeled as a cube root function shape with respect to transmitter antenna height. Moreover, the findings displayed that all system scenarios (except scenario 3 which uses 60 GHz) can properly operate under the influence of either rain or diffraction, not both. In millimeter-wave systems, antenna height as well as the maximum distance that the transmitter can able to appropriately deliver its power to the receiver should be significantly taken into account during the system designing. Furthermore, high sensitive 5G system receivers are recommended particularly during heavy precipitation events operating at a higher frequency spectrum band.

REFERENCES

[1] Y. Wang, T. Zhang, S. Mao, and T. S. Rappaport, "Directional neighbor discovery in mmWave wireless networks," *Digit. Commun. Netw.*, to be published.

[2] J. Baenke, K. R. Chaudhuri, A. Deshpande, A. Halder, M. Irizarry, N. Saxena, S. Sharma, and R. Yang, "Millimeter-wave downlink coverage extension strategies," *IEEE Commun. Mag.*, vol. 58, no. 9, pp. 74–78, Sep. 2020.

[3] J. Huang, Y. Cao, X. Raimundo, A. Cheema, and S. Salous, "Rain statistics investigation and rain attenuation modeling for millimeter wave short-range fixed links," *IEEE Access*, vol. 7, pp. 156110–156120, 2019.

[4] S. Shrestha and D.-Y. Choi, "Characterization of rain specific attenuation and frequency scaling method for satellite communication in South Korea," *Int. J. Antennas Propag.*, vol. 2017, Jan. 2017, Art. no. 8694748.

[5] S. Zang, M. Ding, D. Smith, P. Tyler, T. Rakotoarivelo, and M. A. Kaafar, "The impact of adverse weather conditions on autonomous vehicles: How rain, snow, fog, and hail affect the performance of a self-driving car," *IEEE Veh. Technol. Mag.*, vol. 14, no. 2, pp. 103–111, Jun. 2019.

[6] T. S. Rappaport, S. Sun, R. Mayzus, H. Zhao, Y. Azar, K. Wang, G. N. Wong, J. K. Schulz, M. Samimi, and F. Gutierrez, "Millimeter wave mobile communications for 5G cellular: It will work!" *IEEE Access*, vol. 1, pp. 335–349, 2013.

[7] G. Kizer, *Digital Microwave Communication: Engineering Point-to-Point Microwave Systems*, 1st ed. Hoboken, NJ, USA: Wiley, 2013, p. 222.

[8] Z. A. Shamsan, "Clear air and precipitation millimeter-wave point-to-point wireless link prediction based on terrain path profile in semi-arid climate," *J. Telecommun., Electron. Comput. Eng.*, vol. 10, nos. 2–7, pp. 17–21, 2018.

[9] *Series, R.P. Propagation Data and Prediction Methods Required for the Design of Terrestrial Line-of-Sight Systems*, document Recommendation ITU-R P. 530-12; ITU, Geneva, Switzerland, 2006, pp. 1–47.

[10] *Series, R.P. Propagation Data and Prediction Methods Required for the Design of Terrestrial Line-of-Sight Systems*. document Recommendation ITU-R P. 530-14; ITU, Geneva, Switzerland, 2012, pp. 1–51.

[11] *Series, R.P. Propagation Data and Prediction Methods Required for the Design of Terrestrial Line-of-Sight Systems*. document Recommendation ITU-R P. 530-15; ITU, Geneva, Switzerland, 2013, pp. 1–51.

[12] *Series, R.P. Propagation Data and Prediction Methods Required for the Design of Terrestrial Line-of-Sight Systems*. document Recommendation ITU-R P. 530-16; ITU, Geneva, Switzerland, 2015, pp. 1–56.

[13] S. Shrestha and D.-Y. Choi, "Rain attenuation over terrestrial microwave links in South Korea," *IET Microw., Antennas Propag.*, vol. 11, no. 7, pp. 1031–1039, Jun. 2017.

[14] P. Thorvaldsen and I. Henne, "Outdoor transmission measurement at 26 GHz: Results of a 4 year trial in prague," *Radio Sci.*, vol. 51, no. 5, pp. 402–410, May 2016.

[15] R. M. Islam, Y. A. Abdulrahman, and T. A. Rahman, "An improved ITU-R rain attenuation prediction model over terrestrial microwave links in tropical region," *EURASIP J. Wireless Commun. Netw.*, vol. 2012, no. 1, pp. 1–9, Dec. 2012.

[16] L. A. R. Da. Silva Mello, M. S. Pontes, R. M. De Souza, and N. A. P. Garcia, "Prediction of rain attenuation in terrestrial links using full rainfall rate distribution," *Electron. Lett.*, vol. 43, no. 25, pp. 1442–1443, Dec. 2007.

[17] Z. A. Shamsan, "Dust storm and diffraction modelling for 5G spectrum wireless fixed links in arid regions," *IEEE Access*, vol. 7, pp. 162828–162840, 2019.

[18] G. R. MacCartney, S. Deng, S. Sun, and T. S. Rappaport, "Millimeter-wave human blockage at 73 GHz with a simple double knife-edge diffraction model and extension for directional antennas," in *Proc. IEEE 84th Veh. Technol. Conf. (VTC-Fall)*, Sep. 2016, pp. 1–6.

[19] *Propagation by Diffraction*, document ITU-R P.526-14, 2018.
[20] *Propagation Data and Prediction Methods Required for the Design of Terrestrial Line-of-Sight Systems*, document ITU-R P.530-17, 2017.
[21] Q. Li, G. Li, W. Lee, M.-I. Lee, D. Mazzarese, B. Clerckx, and Z. Li, "MIMO techniques in WiMAX and LTE: A feature overview," *IEEE Commun. Mag.*, vol. 48, no. 5, pp. 86–92, May 2010.
[22] A. Ckalingam, and B. S. Rajan, *Large MIMO Systems*. Cambridge, U.K.: Cambridge Univ. Press, 2014.
[23] N. Hassan and X. Fernando, "Massive MIMO wireless networks: An overview," *Electronics*, vol. 6, no. 3, p. 63, Sep. 2017.
[24] *Fixed Service Use and Future Trends*, document ITU-R F.2323-1, 2017.
[25] *Technical Feasibility of IMT in Bands Above 6 GHz*, document ITU-R M.2376-0, 2015.
[26] *Use of Fixed Service for Transport of Traffic, Including Backhaul, for IMT and Other Terrestrial Mobile Broadband Systems*, document ITU-R F.2393-0, 2016.
[27] M. A. AI-Saleh, "Variability and frequency of daily rainfall in Riyadh, Saudi Arabia," *Geographical Bull.*, vol. 39, no. 1, p. 48, May 1997.
[28] K. R. Jones, O. Berney, D. P. Carr, and E. C. Barrett, *Arid Zone Hydrology for Agricultural Development*, no. 37. Rome, Italy: FAO, 1981.
[29] A. Mashat and H. A. Basset, "Analysis of rainfall over Saudi Arabia," *J. King Abdulaziz Univ.-Meteorol., Environ. Arid Land Agricult. Sci.*, vol. 22, no. 2, pp. 59–78, Jun. 2011.
[30] A. A. Ali, "Reliability analysis of millimeter wave propagation based on long term rain data in riyadh," *Int. J. Infr. Millim. Waves*, vol. 7, no. 4, pp. 599–621, Apr. 1986.
[31] A. A. Ali, M. A. Alhaider, and M. A. Shatila, "Rain map for radiowave propagation design in Saudi Arabia," *Int. J. Infr. Millim. Waves*, vol. 7, no. 11, pp. 1777–1793, Nov. 1986.
[32] M. Almazroui, M. N. Islam, P. D. Jones, H. Athar, and M. A. Rahman, "Recent climate change in the arabian peninsula: Seasonal rainfall and temperature climatology of Saudi Arabia for 1979–2009," *Atmos. Res.*, vol. 111, pp. 29–45, Jul. 2012.
[33] A. A. Ali and M. A. Alhaider, "Effect of multipath fading on millimetre wave propagation: A field study," *IEE Proc. H Microwaves, Antennas Propag.*, vol. 140, no. 5, pp. 343–346, Oct. 1993.
[34] A. A. Ali and M. A. Alhaider, "Millimeter wave propagation in arid land—A field study in riyadh," *IEEE Trans. Antennas Propag.*, vol. 40, no. 5, pp. 492–499, May 1992.
[35] M. C. Kestwal, S. Joshi, and L. S. Garia, "Prediction of rain attenuation and impact of rain in wave propagation at microwave frequency for tropical region (Uttarakhand, India)," *Int. J. Microw. Sci. Technol.*, vol. 2014, Jun. 2014, Art. no. 958498.
[36] I. Osita and E. F. Nymphas, "Characteristics of worst hour rainfall rate for radio wave propagation modelling in Nigeria," *Meteorol. Atmos. Phys.*, vol. 131, no. 2, pp. 251–261, Apr. 2019.
[37] Z. A. Shamsan, "38-GHz point-to-point wireless radio link prediction based on propagation and terrain path profile in riyadh," *Univ. Politehnica Bucharest Sci. Bull., C-Elect. Eng. Comput. Sci.*, vol. 80, no. 1, pp. 121–134, 2018.
[38] C. Kelly, "Nautel's RF toolkit clarifies FM and STL propagation," Broadcasters' Desktop Resource, Montreal, QC, Canada, Tech. Rep., 2012.
[39] *Specific Attenuation Model for Rain for Use in Prediction Methods*, document ITU-R Rec. P.838-1, Geneva, Switzerland, 1999.
[40] *Characteristics of Precipitation for Propagation Modelling*, document Rec. ITU-R P.837-1, Geneva, Switzerland, 1994.
[41] *Characteristics of Precipitation for Propagation Modelling*, document ITU-Rec. P.837-3, Geneva, Switzerland, 2001.
[42] F. Norouzian, E. Marchetti, M. Gashinova, E. Hoare, C. Constantinou, P. Gardner, and M. Cherniakov, "Rain attenuation at millimeter wave and low-THz frequencies," *IEEE Trans. Antennas Propag.*, vol. 68, no. 1, pp. 421–431, Jan. 2020.
[43] J. S. Seybold, *Introduction to RF Propagation*, 2nd ed. Hoboken, NJ, USA: Wiley, 2005.
[44] W. C. Y. Lee, *Mobile Communication Engineering, Theory and Applications*, 2nd ed. New York, NY, USA: McGraw-Hill, 1998, p. 142.
[45] Y. Zhang, M. Roughan, C. Lund, and D. L. Donoho, "Estimating point-to-point and point-to-multipoint traffic matrices: An information-theoretic approach," *IEEE/ACM Trans. Netw.*, vol. 13, no. 5, pp. 947–960, Oct. 2005.
[46] Z. A. Shamsan, M. Alammar, A. Alharthy, A. Aldahmash, K. A. Al-Snaie, and A. M. Al-Hetar, "Micrometer and millimeter wave P-to-P links under dust storm effects in arid climates," *Eng., Technol. Appl. Sci. Res.*, vol. 9, no. 4, pp. 4520–4524, Aug. 2019.
[47] A. M. Al-Samman, M. H. Azmi, Y. A. Al-Gumaei, T. Al-Hadhrami, T. A. Rahman, Y. Fazea, and A. Al-Mqdashi, "Millimeter wave propagation measurements and characteristics for 5G system," *Appl. Sci.*, vol. 10, no. 1, p. 335, Jan. 2020.
[48] A. Al-Saman, M. Mohamed, M. Cheffena, M. H. Azmi, and T. A. Rahman, "Performance of full-duplex wireless back-haul link under rain effects using E-Band 73 GHz and 83 GHz in tropical area," *Appl. Sci.*, vol. 10, no. 17, p. 6138, Sep. 2020.
[49] A. M. Al-Saman, M. Cheffena, M. Mohamed, M. H. Azmi, and Y. Ai, "Statistical analysis of rain at millimeter waves in tropical area," *IEEE Access*, vol. 8, pp. 51044–51061, 2020.
[50] T. S. Rappaport, Y. Xing, G. R. MacCartney, A. F. Molisch, E. Mellios, and J. Zhang, "Overview of millimeter wave communications for fifth-generation (5G) wireless networks—With a focus on propagation models," *IEEE Trans. Antennas Propag.*, vol. 65, no. 12, pp. 6213–6230, Dec. 2017.
[51] A. M. Al-Samman, M. Mohamed, Y. Ai, M. Cheffena, M. H. Azmi, and T. A. Rahman, "Rain attenuation measurements and analysis at 73 GHz E-band link in tropical region," *IEEE Commun. Lett.*, vol. 24, no. 7, pp. 1368–1372, Jul. 2020.
[52] C. Han, J. Huo, Q. Gao, G. Su, and H. Wang, "Rainfall monitoring based on next-generation millimeter-wave backhaul technologies in a dense urban environment," *Remote Sens.*, vol. 12, no. 6, p. 1045, Mar. 2020.
[53] M. Agiwal, A. Roy, and N. Saxena, "Next generation 5G wireless networks: A comprehensive survey," *IEEE Commun. Surveys Tuts.*, vol. 18, no. 3, pp. 1617–1655, 3rd Quart., 2016.
[54] H. Xu, T. S. Rappaport, R. J. Boyle, and J. H. Schaffner, "Measurements and models for 38-GHz point-to-multipoint radiowave propagation," *IEEE J. Sel. Areas Commun.*, vol. 18, no. 3, pp. 310–321, Mar. 2000.
[55] *Attenuation by Atmospheric Gases*, document ITU-R 1-676, Sep. 2016.
[56] Y. Xing and T. S. Rappaport, "Propagation measurement system and approach at 140 GHz-moving to 6G and above 100 GHz," in *Proc. IEEE Global Commun. Conf. (GLOBECOM)*, Dec. 2018, pp. 1–6.
[57] C. T. Phillips, "Geostatistical techniques for practical wireless network coverage mapping," Ph.D. dissertation, Univ. Colorado Boulder, Boulder, CO, USA, 2012.
[58] *Conditions for the Coexistence Between Fixed Service and Other Envisaged Outdoor Uses/Applications in the 57-66 GHz Range*, document ECC Rep. 288, 2019.
[59] S. Shrestha and D.-Y. Choi, "Rain attenuation statistics over millimeter wave bands in South Korea," *J. Atmos. Solar-Terrestrial Phys.*, vols. 152–153, pp. 1–10, Jan. 2017.
[60] I. Shayea, T. A. Rahman, M. H. Azmi, and M. R. Islam, "Real measurement study for rain rate and rain attenuation conducted over 26 GHz microwave 5G link system in Malaysia," *IEEE Access*, vol. 6, pp. 19044–19064, 2018.
[61] S. Chakraborty, M. Chakraborty, and S. Das, "Experimental studies of slant-path rain attenuation over tropical and equatorial regions: A brief review," *IEEE Antennas Propag. Mag.*, early access, Mar. 24, 2020, doi: 10.1109/MAP.2020.2976911.
[62] T. S. Rappaport, *Wireless Communications: Principles and Practice*, 2nd ed. Upper Saddle River, NJ, USA: Prentice-Hall, 2002.

ZAID AHMED SHAMSAN (Senior Member, IEEE) received the B.Sc. (Hons.) degree in electronics and communication engineering from the Sudan University of Sciences and Technology (SUST), in 2002, and the master's and Ph.D. degrees in telecommunication and electrical engineering from Universiti Teknologi Malaysia (UTM), Johor, Malaysia, in 2007 and 2010, respectively.

He was a Postdoctoral Research Fellow with the Wireless Communication Center (WCC), Faculty of Electrical Engineering, UTM, from April 2010 to April 2012. Since 2003, he has been with Taiz University, Taiz, Yemen. He is currently an Associate Professor with the Department of Electrical Engineering, College of Engineering, Al Imam Mohammad Ibn Saud Islamic University, Riyadh, Saudi Arabia. He has published several scientific papers in high impact factor and archival technical journals and conferences. His research interests include orthogonal frequency-division multiplexing technology, interference analysis techniques, mathematical modeling for coexistence analysis in wireless networks, wave propagation, rainfall and dust storm analysis and mitigation, free space optics, and optical communication.